NOSC

Technical Report 184

ADAPTIVE NOISE CANCELLING AND ENHANCEMENT OF A SINUSOID IN UNCORRELATED NOISE

EH Satorius

1 December 1977

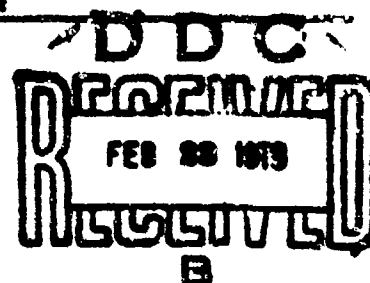Research and Development: August-November 1977

Prepared For
Chief of Naval Operations

**NAVAL OCEAN SYSTEMS CENTER
SAN DIEGO, CALIFORNIA 92152**

DDC

RECEIVED

FEB 28 1978

B

NAVAL OCEAN SYSTEMS CENTER, SAN DIEGO, CA 92152

AN ACTIVITY OF THE NAVAL MATERIAL COMMAND

RR GAVAZZI, CAPT USN
Commander

HL BLOOD
Technical Director

ADMINISTRATIVE INFORMATION

Released by
RH Hearn, Head
Electronics Division

Under authority of
DA Kunz, Head
Fleet Engineering Department

REPORT DOCUMENTATION PAGE		READ INSTRUCTIONS BEFORE COMPLETING FORM
1. REPORT NUMBER NOSC TR 184	2. GOVT ACCESSION NO.	3. RECIPIENT'S CATALOG NUMBER
4. TITLE (and Subtitle) ADAPTIVE NOISE CANCELLING AND ENHANCEMENT OF A SINUSOID IN UNCORRELATED NOISE		5. TYPE OF REPORT & PERIOD COVERED Research and Development (R&D) August – November 1977
		6. PERFORMING ORG. REPORT NUMBER
7. AUTHOR(s) E. H. Satorius		8. CONTRACT OR GRANT NUMBER(s)
9. PERFORMING ORGANIZATION NAME AND ADDRESS Naval Ocean Systems Center San Diego, CA 92152		10. PROGRAM ELEMENT, PROJECT, TASK AREA & WORK UNIT NUMBERS PE61015N
11. CONTROLLING OFFICE NAME AND ADDRESS Chief of Naval Operations		12. REPORT DATE 1 December 1977
		13. NUMBER OF PAGES 53
14. MONITORING AGENCY NAME & ADDRESS(if different from Controlling Office)		15. SECURITY CLASS (of this report) UNCLASSIFIED
		15a. DECLASSIFICATION DOWNGRADING SCHEDULE

16. DISTRIBUTION STATEMENT (of this Report)

Approved for public release; distribution unlimited.

17. DISTRIBUTION STATEMENT (of the abstract entered in Block 20, if different from Report)

18. SUPPLEMENTARY NOTES

19. KEY WORDS (Continue on reverse side if necessary and identify by block number)

20. ABSTRACT (Continue on reverse side if necessary and identify by block number)

The response of the adaptive line canceller and enhancer (ALICE) processor to inputs which contain sinusoidal interferences in uncorrelated noise is examined. It is found that under certain conditions the steady-state output power spectrum of ALICE will contain peaks at the frequencies of the interfering sinusoids. In general, the growth time of these peaks is much longer than the ALICE's response time to a signal. However, once the peaks appear at the interference frequencies, their presence may interfere with the detection of other signal peaks in

DD FORM 1473 EDITION OF 1 NOV 65 IS OBSOLETE

393 159

20. (Continued)

the output power spectrum. Therefore, different methods of eliminating these peaks are examined: increasing the ALE delay, increasing the ANC notch widths, and adding uncorrelated noise to the ALE input. Experimental data that indicate the validity of these analyses are included.

SUMMARY

PROBLEM

Examine the response of the adaptive line canceller and ennancer (ALICE) processor to inputs which contain sinusoidal interference in uncorrelated noise.

RESULTS

It was found that under certain conditions the steady-state output power spectrum of ALICE contains peaks at the frequencies of the interfering sinusoids. The growth time of these peaks is generally much longer than the ALICE's response time to a signal. Once these peaks appear at the interference frequencies, their presence can interfere with the detection of other signal peaks in the output power spectrum.

Different methods of eliminating these peaks were examined:

1. Increasing the ALE delay to decorrelate the notch

2. Increasing the notch width

3. Adding uncorrelated noise to the ALE input

Experimental data were generated to indicate the validity of these analyses.

1

CONTENTS

2

INTRODUCTION

It is frequently of interest to detect the presence of narrowband signals which are corrupted by broadband noise and narrowband interferences. Since the center frequencies of the signals and the narrowband interferences may not be known precisely and may possibly drift, bandpass and notch filters, whose frequency response characteristics can continually adapt to provide simultaneous adaptive enhancement of the signals and adaptive cancellation of the narrowband interferences, are of interest.

A promising implementation of such an adaptive processor uses the Widrow-Hoff LMS algorithm, and consists of an adaptive noise canceller (ANC) followed by an adaptive line enhancer (ALE) (references 1 through 4). This implementation (figure 1) is referred to as an adaptive line canceller and enhancer (ALICE) processor (references 5 and 6). The primary input to ALICE, $x(j)$, consists of narrowband signals as well as broadband and narrowband noise; the reference input to ALICE, $x_r(j)$, consists of narrowband components at all frequencies where narrowband interference is expected to occur. In general, the primary input will contain interference at some, but not all, frequencies present in the reference input. The output of the ANC, $q(j)$, is narrowband signals, broadband noise, and notches at the frequencies of the narrowband components in the reference input. A typical plot of the power spectral densities of $x(j)$, $S_x(\omega)$ and $q(j)$, $S_q(\omega)$ is in figure 2.

primary
input, $x(j)$

reference
input, $x_r(j)$

adaptive
noise
canceller
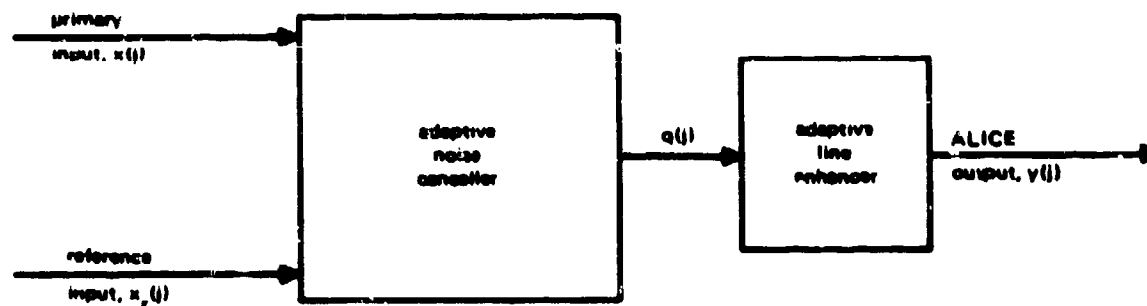
$q(j)$

adaptive
line
enhancer

ALICE
output, $y(j)$

Figure 1. ALICE processor.

The output of the ALE and ALICE, $y(j)$, ideally consists only of the narrowband signals. In practice, however, two factors connected with the ALE prevent ALICE from attaining its ideal performance. The first factor, the weight vector noise occurring in the ALE, arises from gradient estimation errors in the Widrow-Hoff LMS algorithm (references 2 and 7). (The effects of weight vector noise on the power spectral density of $y(j)$, $S_y(\omega)$ are discussed in more detail on pages 22 to 25.) The second factor is more fundamental and is directly related to the basic goal of the ALE. As discussed by a number of authors (references 3, 4, 8, 9, 10, 11, and 12), the ALE is an adaptive implementation of a linear
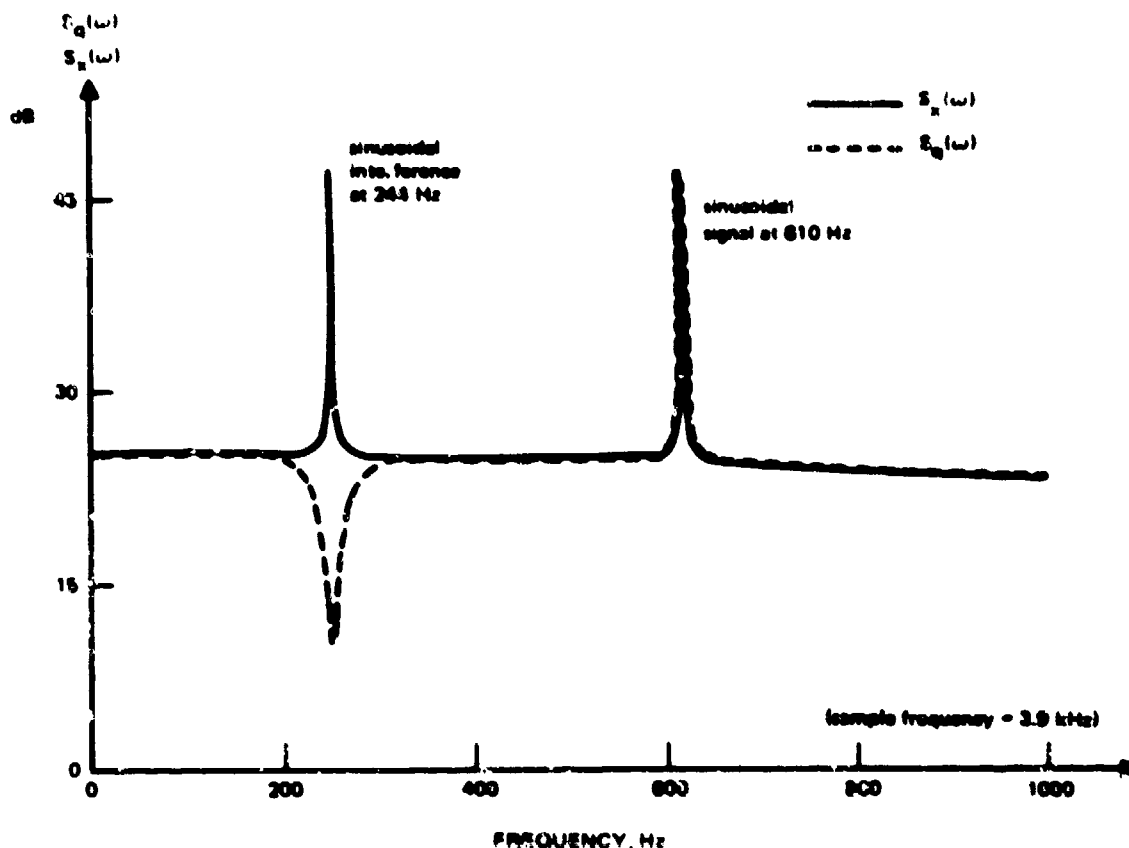
Figure 2. Plot of the ANC input and output power spectra, $S_x(\omega)$ and $S_0(\omega)$, respectively. The rms voltages of the input signal, interference, and noise were 0.6, 0.6, and 1.0 V, respectively. (Data were obtained from a hardware implementation of ALICE (built at NOSC) using a 256-weight ANC and a 256-weight ALE.)

prediction filter which attempts to estimate the input Δ steps into the future. (The prediction distance Δ is referred to as the bulk delay of the ALE.) Therefore, the basic goal is prediction. When the input to the ALE consists of sinusoidal signals in noise, which has an approximately flat power spectral density, the goal of prediction is consistent with forming bandpass filters at the sinusoid frequencies (references 2, 3, 4, and 11). Therefore, the ALE effectively filters the noise from the signals for these cases. However, when the background noise is not a flat power spectrum, the behavior of the ALE can depart drastically from simple bandpass filtering at the signal frequencies. In particular, when the power spectrum of the input background noise contains notches which have been created as a result of cancelling narrowband interferences, as in the case of the ALICE processor, the ALE output power spectrum may contain undesired peaks at the frequencies of the notches. This is clearly seen in figure 3 where the output power spectrum of the ALE,

4

$S_y(\omega)$, is plotted in accordance with the input power spectrum, $S_q(\omega)$, in figure 2. The enhanced signal is clearly evident in the ALE output and a peak is also evident at the frequency of the notch. The presence of this peak is a consequence of the behavior of linear prediction filters to input spectra which contain notches or zeroes.
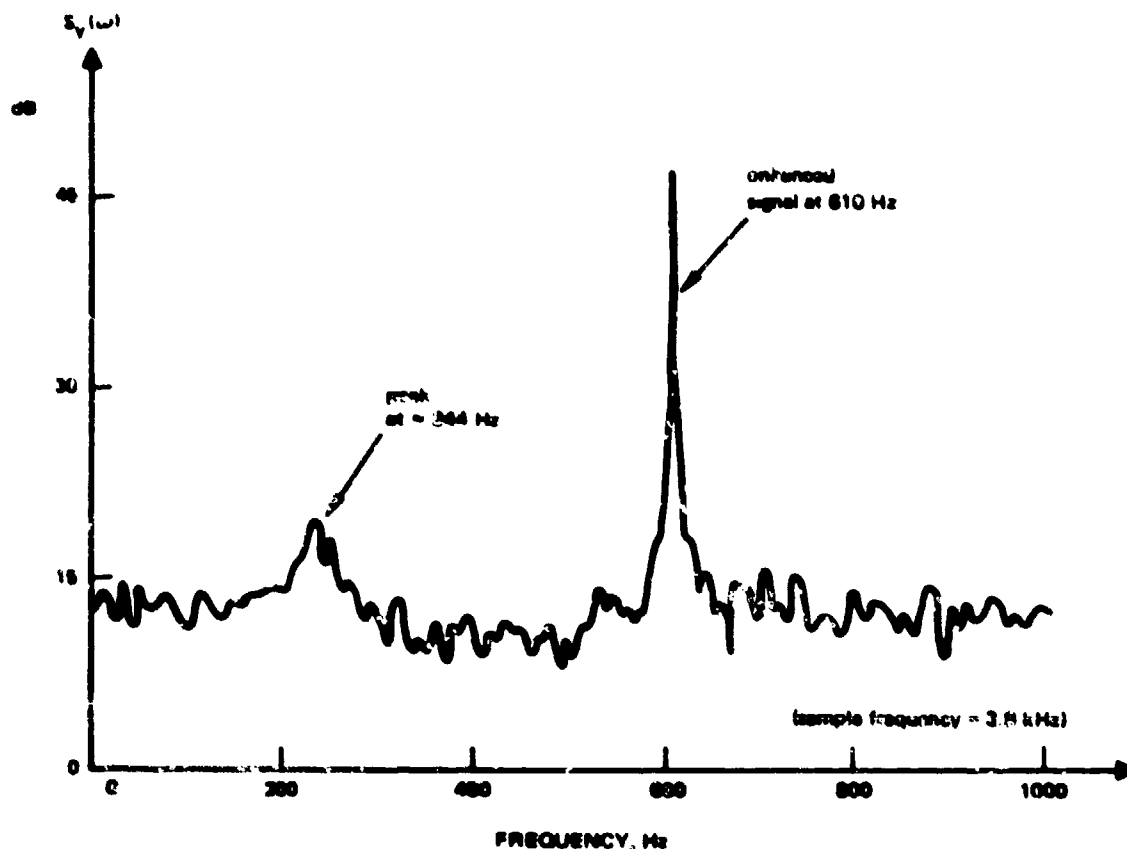

Figure 3. Plot of the ALE output power spectrum, $S_y(\omega)$, when the input power spectrum contains a notch and the ALE responds to the notch. (All parameters are as in figure 2.)

It is the purpose of this report to examine analytically and experimentally the response of ALICE to input spectra which contain sinusoidal interferences in uncorrelated noise. In particular, it is shown in the next section that when sinusoidal interferences are present in the primary input to ALICE the ANC responds by forming a notch at the frequency of the interference, which can, in turn, produce undesirable peaks in the power spectrum of the ALICE output at the frequencies of the notches. It is also shown analytically and experimentally that the generation of these peaks in the ALE output can be prevented by proper selection of ALE and ANC parameters.

5

RESPONSE OF ALICE PROCESSOR TO SINUSOIDAL INTERFERENCE IN UNCORRELATED NOISE

ANC RESPONSE TO SINUSOIDAL INTERFERENCE

As previously discussed, the ALICE processor is usually faced with the task of simultaneously cancelling narrowband interferences and enhancing narrowband signals which are immersed in broadband noise. In this section, we will be primarily concerned with the noise-cancelling capabilities of ALICE. In particular, the power spectral density of the ALICE output, $S_y(\omega)$, will be derived when the primary input to ALICE, $x(j)$, contains an interfering sinusoid as well as uncorrelated noise. The reference input, $x_r(j)$, is assumed to contain a noise-free copy of the interfering sinusoid. The case where signals are also present in the primary input will not be treated in this report.*

To examine the ALICE output power spectrum, the response of the ANC to a sinusoidal interference in broadband noise must first be determined. Glover (reference 1) has given a complete analytical treatment of the ANC response when $x_r(j)$ contains a noise-free copy of the interfering sinusoid, i.e., when

$$x_r(j) = C \cos \omega_r j. \tag{1}$$

In equation (1), ω_r represents the frequency of the interfering sinusoid (normalized to the sample frequency, i.e., $\omega_r = 2\pi f_r T$, where f_r is the sinusoid frequency in hertz and T is the sampling interval in seconds) and C is the amplitude of the interfering sinusoid. Glover has shown that to a good approximation the ANC will form a narrow notch filter with the transfer function, $H_{ANC}(z)$ (from x to q in figure 1), given by

$$H_{ANC}(z) = \frac{(z - e^{j\omega_r})(z - e^{-j\omega_r})}{(z - z_0)(z - \bar{z}_0)} \tag{2}$$

where

$$z_0 \approx e^{-\beta + j\omega_r} \tag{3}$$

and

$$\beta \approx \mu_{ANC} \frac{C^2}{2}. \tag{4}$$

---

*If the signal frequencies are separated by at least the filter resolution of the ALE, ALICE will, to a good approximation, respond independently to the signals. For a more complete treatment of the ALE response to multiple signals in broadband noise, refer to references 3 and 11.

6

In equation (4), N is the number of ANC filter weights and μ_{ANC} is the adaptation constant of the ANC (references 1 and 2). The digital frequency response of the ANC can be found by plotting $|H_{ANC}(e^{j\omega})|$ for values of ω from 0 to π. A typical plot of $|H_{ANC}|$ is presented in figure 4. It is important to note (equation (2)) that for a noise-free sinusoidal reference the frequency response of the ANC equals zero at $\omega = \pm\omega_r$, i.e.,
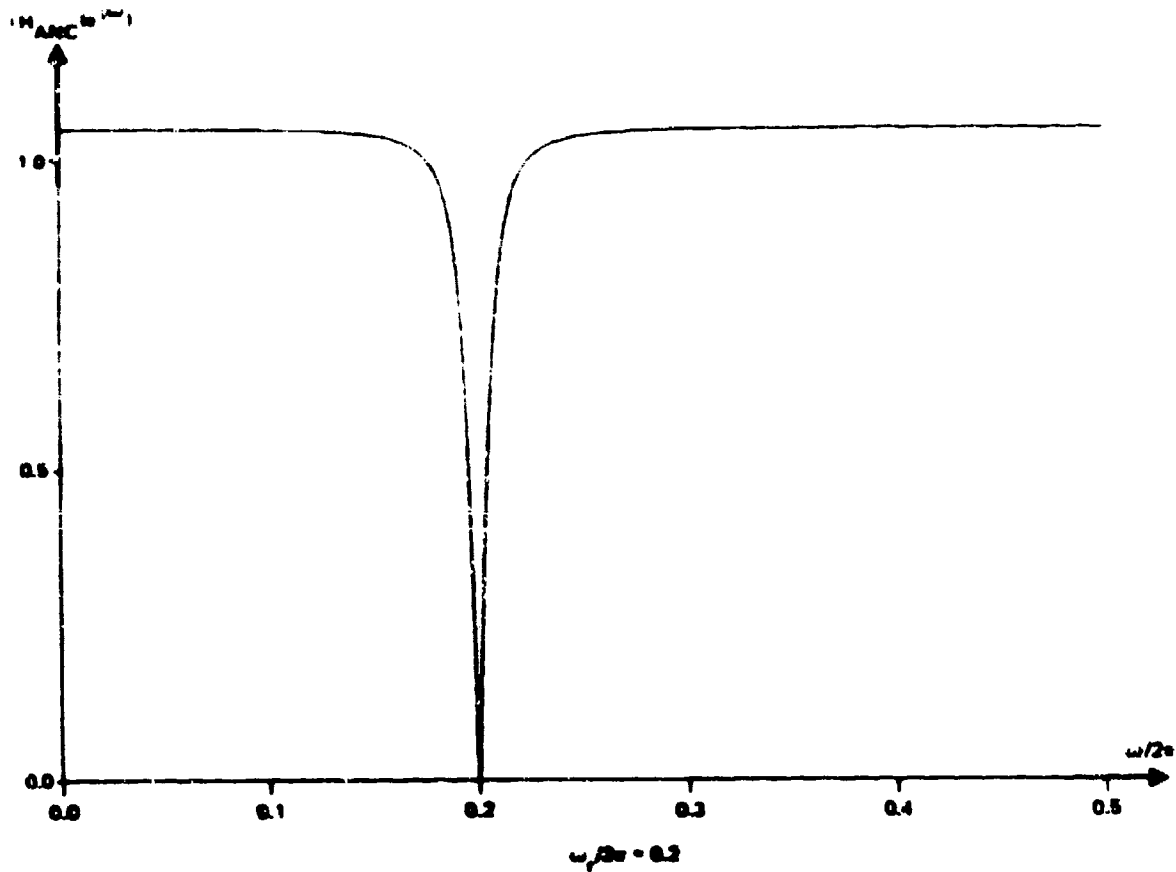
$$|H_{ANC}(e^{\pm j\omega_r T})| = 0 \tag{5}$$

Figure 4. Theoretical plot of the digital frequency response of the ANC for $\mu_{ANC} = 0.05$, $C = 1$, and $N = 2$.

The power spectral density of the ANC output and the ALE input, $S_q(\omega)$, is given by

$$S_q(\omega) = S_x(\omega) |H_{ANC}(e^{j\omega})|^2 . \tag{6}$$

For the case of sinusoidal interference and uncorrelated noise in the primary input, $S_x(\omega)$ is given by

$$S_x(\omega) = \sigma_0^2 + \frac{\sigma_s^2}{2} \left[\delta(\omega - \omega_r) + \delta(\omega + \omega_r) \right]. \tag{7}$$

In equation (7), σ_0^2 is the white noise power, σ_s^2 represents the power of the sinusoidal interference in the primary channel, and $\delta(\cdot)$ represents a Dirac delta function which has the following properties (reference 13):

$$\int_C \delta(x - x_0) \phi(x) \, dx = \phi(x_0) \tag{8}$$

and

$$\phi(x) \, \delta(x - x_0) = \phi(x_0) \, \delta(x - x_0). \tag{9}$$

In equations (8) and (9), $\phi(x)$ is any function that is continuous at $x = x_0$ and C is any interval that contains the point $x = x_0$. From equations (5), (6), (7), and (9), the power spectral density of the ALE input is given by

$$S_q(\omega) = \sigma_0^2 \, |H_{ANC}(e^{j\omega})|^2. \tag{10}$$

Equation (10) shows that, if there is perfect ANC cancellation at $\omega = \omega_r$, the input power spectrum to the ALE will consist of a notched noise spectrum. A typical plot of $S_q(\omega)$ is in figure 5. Because of noise sources such as quantization, $|H_{ANC}(e^{\pm j\omega_r}|$ will not exactly equal zero and, therefore, the ANC will not completely cancel the interfering sinusoid. However, in most situations, such a small amount of the interference gets through to the ANC output that equation (10) provides a good approximation to the ALE input power spectrum.

ALE RESPONSE TO NOTCHED INPUT NOISE SPECTRUM: WIENER SOLUTION

As previously discussed, the ALE is an adaptive implementation of a linear predictive filter. The ALE uses the Widrow-Hoff LMS algorithm to update continually its filter weights (reference 8):

$$w_k(i + 1) = w_k(i) + 2\mu_{ALE} \, [q(i) \, q \, (i - \Delta - k)$$

$$\tag{11}$$

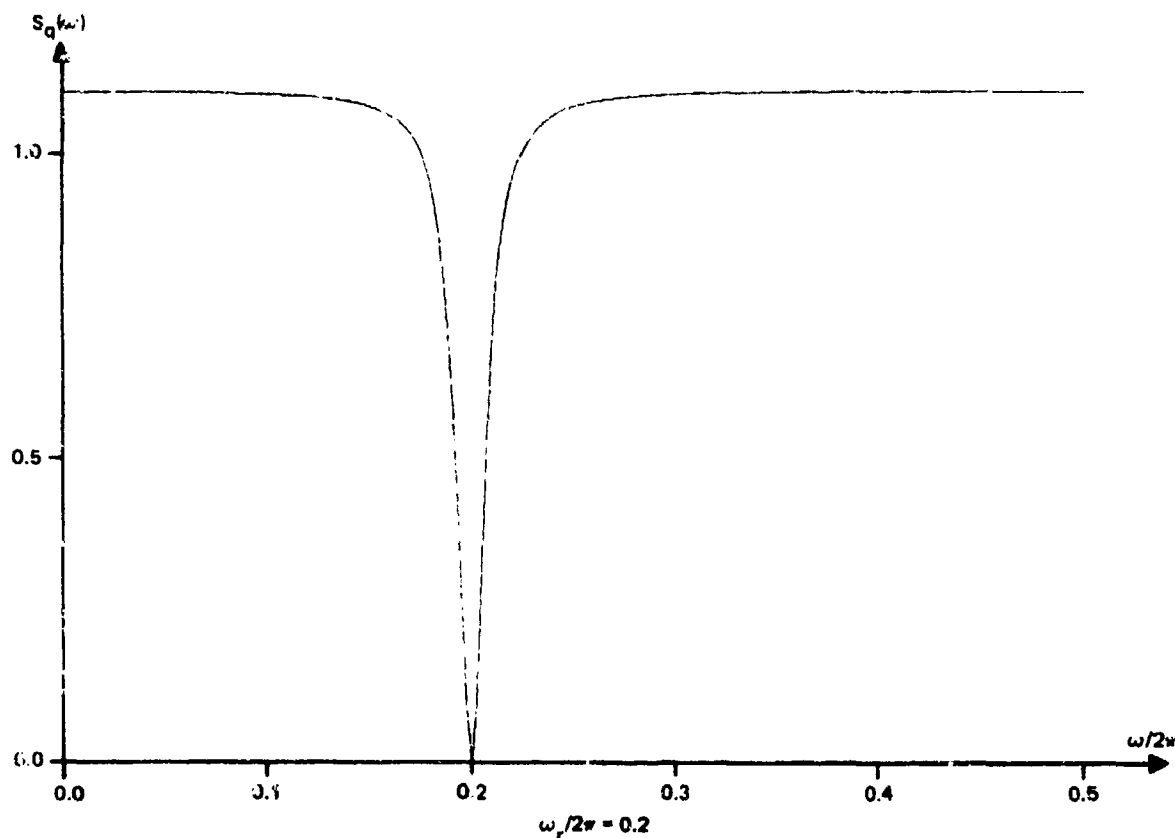$$- q(i - \Delta - k) \sum_{\ell = 0}^{L - 1} q(i - \Delta - \ell) \, w_j(i)], \quad k = 0, 1, \ldots, L - 1$$

Figure 5. Theoretical plot of the ALE input power spectrum, $S_q(\omega)$, for $\sigma_0^2 = 1.0$ and $\beta = 0.05$.

where $w_k(j)$ is the $j\underline{th}$ update of the $k\underline{th}$ weight of the ALE, μ_{ALE} is the adaptation constant of the ALE, and L and Δ are, respectively, the number of ALE weights and the ALE delay (or prediction distance). (A number of the properties of equation (11) is discussed in references 2 through 4 and 7 through 12.) The particular property of equation (11) which is needed in this section concerns convergence. In particular, it has been shown in references 8, 9, and 14 that for uncorrelated stationary inputs the expected value of $w_k(j)$ converges to the solution of the Wiener-Hopf matrix equation, if $0 \le \mu_{ALE} < 1/\lambda_{max}$, where λ_{max} is the largest eigenvalue of the data autocorrelation matrix:

$$\lim_{j \to \infty} E[w_k(j)] = w_k^*, \quad k = 0, 1, \ldots, L-1 . \tag{12}$$

In equation (12) $E[\cdot]$ denotes expectation and w_k^* is the $k\underline{th}$ component of the L-dimensional vector $\underset{\sim}{W}^*$, which is the solution of the Wiener-Hopf matrix-equation:

$$\underset{\sim}{R} \cdot \underset{\sim}{W}^* = \underset{\sim}{P} . \tag{13}$$

In equation (13) $\underset{\sim}{R}$ is the L × L data autocorrelation matrix with elements $(\underset{\sim}{R})_{\ell k} = \rho(\ell - k)$, where $\rho(\ell) = E[q(j)q(j + \ell)]$ is the autocorrelation function for $q(j)$, and $\underset{\sim}{P}$ is the L-dimensional vector with components $(\underset{\sim}{P})_k = \rho(k + \Delta)$. It is noted that $\rho(\ell)$ may be obtained from $S_q(\omega)$ through the transformation

9

$$\rho(\ell) = \frac{1}{2\pi} \int_{-\pi}^{\pi} S_q(\omega) e^{j\omega\ell} d\omega . \tag{14}$$

Since the power spectral density of q in equation (10) will closely resemble that of uncorrelated noise, the uncorrelated property of q(j) is a good assumption, if $\beta \ll 1$. Therefore, the analysis of equation (13) will provide a good description of the mean steady-state behavior of the ALE. The effects of weight vector noise, as well as the transient behavior of the ALE for a stationary input with a power spectrum given by equation (10), are discussed on pages 22 through 25.

An analytical technique which can be used to solve equation (13) is discussed in reference 15. However, before directly applying this technique to equation (13) with $\rho(\ell)$ given by equations (14) and (10), it is useful to replace $S_q(\omega)$ in equation (14) with $S_q^c(\omega)$:

$$S_q^c(\omega) = \sigma_0^2 \frac{(e^{j\omega} - e^{j\omega_r})(e^{-j\omega} - e^{-j\omega_r})}{(e^{j\omega} - e^{j\omega_r - \beta})(e^{-j\omega} - e^{-j\omega_r - \beta})}$$

$$= \sigma_0^2 e^\beta \frac{1 - \cos(\omega_r - \omega)}{\cosh\beta - \cos(\omega_r - \omega)} . \tag{15}$$

A typical plot of $S_q^c(\omega)$ is in figure 6. A comparison of figures 5 and 6 shows that, if ω_r is not too close to zero and if $\beta \ll 1$, $S_q^c(\omega)$ is a good approximation to $S_q(\omega)$ for $\omega > 0$. The solution of equation (13) for w_k^* with $S_q(\omega)$ in equation (14) replaced by $S_q^c(\omega)$ is much more amenable to analysis than when $\rho(\ell)$ is computed directly from equation (14). Furthermore, since $S_q^c(\omega)$ is a good approximation to $S_q(\omega)$ (especially in the vicinity of $\omega \approx \omega_r$), it is expected that the behavior of $|H^*(\omega)|$ near $\omega \approx \omega_r$, where

$$H^*(\omega) \equiv \sum_{k=0}^{L-1} e^{-j\omega(k+1)} w_k^* , \tag{16}$$

can be described to a good approximation when $S_q^c(\omega)$ is used to compute $\rho(\ell)$. Therefore, to gain insight into the steady-state behavior of the ALE for a notched input noise spectrum, we will consider the solution of equation (13) when $\rho(\ell)$ is derived from equation (14) with $S_q(\omega)$ replaced by equation (15).

For this case, $\rho(\ell)$ is given by

$$\rho(\ell) = \frac{1}{2\pi} \int_{-\pi}^{\pi} S_q^c(\omega) e^{j\omega\ell} d\omega$$

$$= \sigma_0^2 e^\beta \left\{ \delta(\ell) - \frac{\cosh\beta - 1}{\sinh\beta} e^{-\beta|\ell| + j\omega_r\ell} \right\} . \tag{17}$$
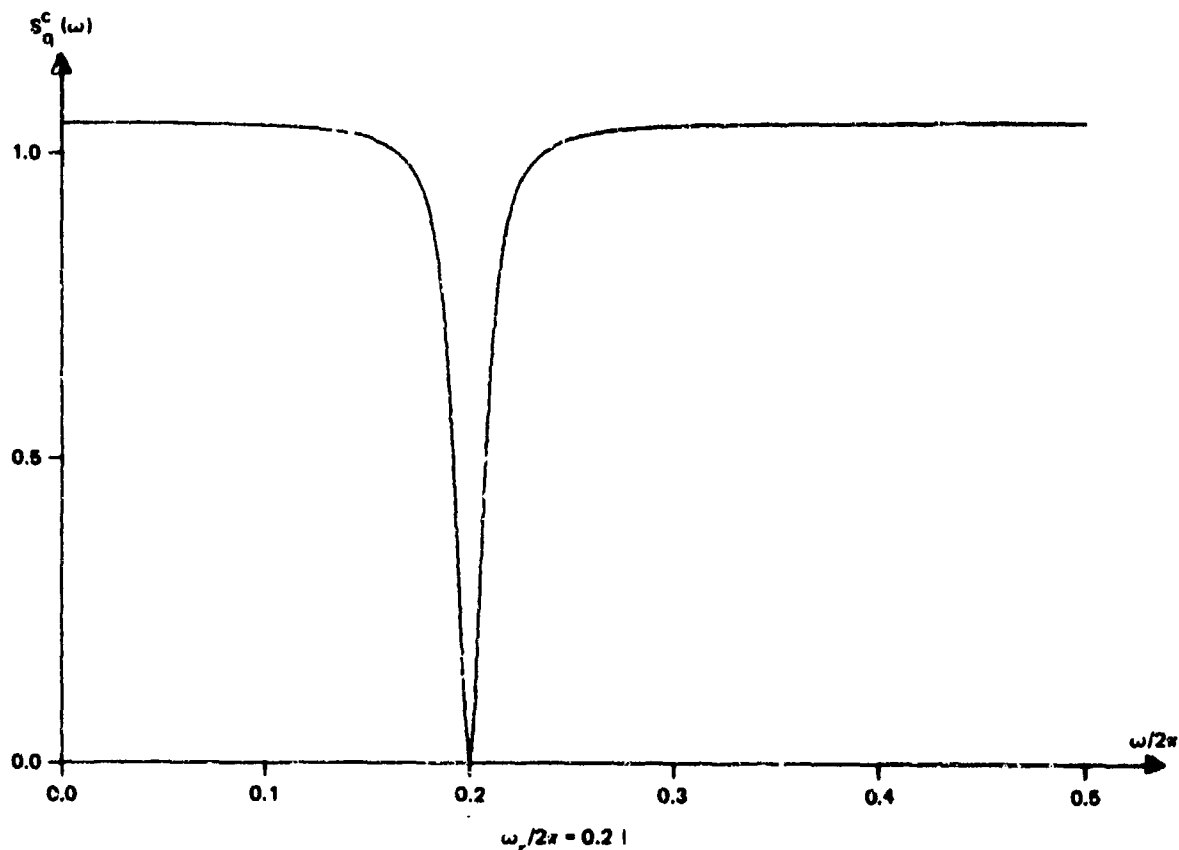
Figure 6. Plot of the approximation, $S_q^c(\omega)$, to the true ALE input power spectrum. $\sigma_0^2 = 1.0$ and $\beta = 0.05$.

Equation (13) can now be solved by the method of undetermined coefficients (reference 15). In particular, since $S_q^c(\omega)$ has two zeroes, both at $\omega = \omega_r$ (as seen in equation (15)), we can assume a solution for w_k^* (corresponding to the treatment in reference 15):

$$w_k^* = Ae^{j\omega_r k} + Bke^{j\omega_r k} . \qquad (18)$$

The constants A and B can be determined by substitution of equation (18) into equation (13). The result is

$$
\left.\begin{array}{l}
A = \dfrac{-2(1 - \cosh\beta)^2\, e^{-\beta\Delta + j\omega_r\Delta}}{(L(\cosh\beta - 1) + \sinh\beta)(1 - e^{-\beta})^2}\,(e^{-\beta} + L(1 - e^{-\beta})) \\[4mm]
B = \dfrac{2(1 - \cosh\beta)^2\, e^{-\beta\Delta + j\omega_r\Delta}}{(L(\cosh\beta - 1) + \sinh\beta)(1 - e^{-\beta})}
\end{array}\right\} . \qquad (19)
$$

For $\beta \ll 1$, equation (18) is given to a good approximation by

$$w_k^* \approx -\frac{\beta}{2}\frac{e^{-\beta\Delta + j\omega_r\Delta}}{(L\beta/2) + 1}\left\{(\beta(L - 1) + 1)e^{j\omega_r k} - \beta ke^{j\omega_r k}\right\}, \beta \ll 1 . \quad (20)$$

11

Equation (20) is the expression for the impulse response of the Wiener filter to a notched input spectrum given by equation (15). To obtain a better perspective on the implication of equation (20), the square of the frequency response, $|H^*(\omega)|^2$, must be examined. From equations (16) and (20) we have

$$|H^*(\omega)|^2 = \frac{\beta^2}{4} \frac{e^{-2\beta\Delta}}{\{(L\beta/2)+1\}^2} \left\{ \left(\frac{\beta}{2}(L-1)+1\right)^2 \phi_L^2(\omega_r - \omega) \right.$$
$$\left. + \beta^2 \left[\phi_L'(\omega_r - \omega)\right]^2 \right\} , \beta \ll 1 \tag{21}$$

where

$$\phi_L(\omega) = \begin{cases} \dfrac{\sin \omega L/2}{\sin \omega/2} & ; \quad \omega \neq 0 \\[2mm] L & ; \quad \omega = 0 \end{cases} \tag{22}$$

and

$$\phi_L'(\omega) \equiv \frac{d\phi_L}{d\omega} = \begin{cases} \dfrac{L \cos \omega L/2 \sin \omega/2 - \sin \omega L/2 \cos \omega/2}{2 \sin^2 \omega/2} & ; \omega \neq 0 \\[2mm] 0 & ; \omega = 0. \end{cases} \tag{23}$$

Equation (21) may be further simplified for $L \gg 1$:

$$|H^*(\omega)|^2 \cong \frac{\beta^2}{4} e^{-2\beta\Delta} \left\{ \phi_L^2(\omega_r - \omega) + \left(\frac{1}{2}+\beta^{-1}\right)^{-2} [\phi_L'(\omega_r - \omega)]^2 \right\} \tag{24}$$

$$\beta \ll 1 ; L \gg 1.$$

The conditions $\beta \ll 1$ and $L \gg 1$ are excellent approximations for the purposes of this study and will therefore be assumed in the subsequent formulae. In figure 7, a typical plot of $|H^*(\omega)|^2$ from equation (24) is shown. Also, for sake of comparison, a plot of $|H^*(\omega)|^2$, calculated using the real autocorrelation function, $\rho(\ell)$, derived from $S_q(\omega)$, is also shown. As expected, there is little difference between the two plots in the vicinity of $\omega = \omega_r$. An interesting feature in figure 7 is the very large peak value of $|H^*(\omega)|^2$ at the notch frequency. The limiting value of this peak for large L is given by

$$|H^*(\omega_r)|^2 = \frac{\beta^2}{4} \cdot e^{-2\beta\Delta} L^2 \tag{25}$$

(from equation (24)). Equation (25) shows that the square of the frequency response of a linear prediction filter to a notched input spectrum increases with L^2 at the frequency of the notch. This result is in drastic contrast to the frequency response of a linear prediction filter to an input spectrum with a sinusoid and broadband noise. in the latter case, the limiting value of the frequency response at the sinusoid frequency approaches 1 for large L (references 3, 4, 9, 10, and 11).
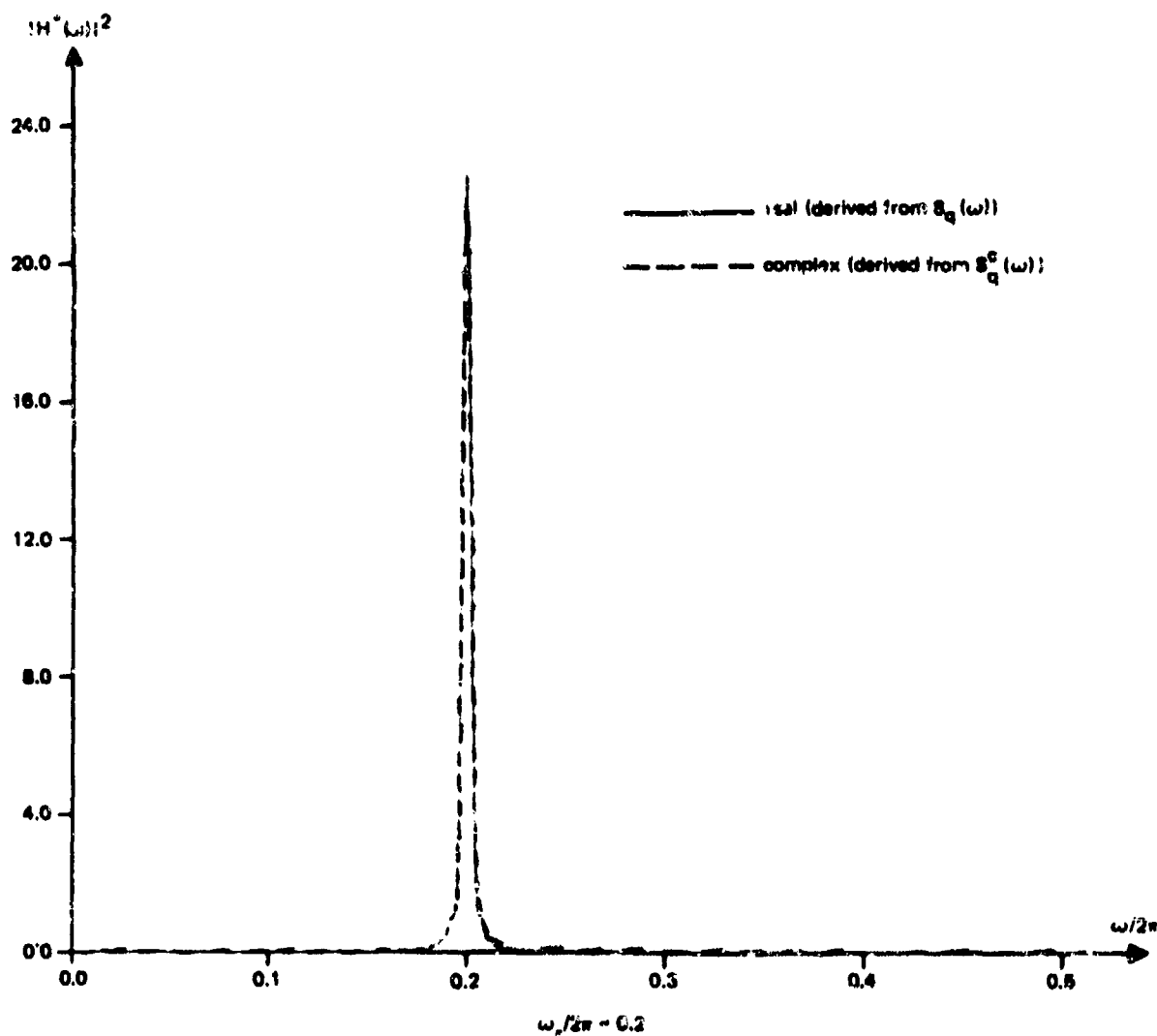
Figure 7. Theoretical plot of the square of the averaged, steady-state ALE frequency response (corresponding to both complex and real autocorrelation functions for the ALE input, $\varphi(\Omega)$). $\beta = 0.05$, $L = 200$, and $\Delta = 1$.

These two quite different responses of linear prediction filters to notches and sinusoids can be understood intuitively from the "whitening" filter interpretation of a linear prediction filter. Briefly, it has been shown, e.g., reference 16, that when $\Delta = 1$ the error output sequence from a linear prediction filter, which is the input sequence less the output sequence from the prediction filter, is approximately uncorrelated in the limit of large L. Therefore, the power spectrum of the prediction filter error sequence is approximately flat. Peacock and Treitel (reference 16) have shown that when L is large and $\Delta = 1$

$$|1 - H^a(\omega)|^2 = \frac{\xi_{min}}{S(\omega)} \quad , \tag{26}$$

13

where ξ_{min} is the minimum-mean-square error of the prediction filter and $S(\omega)$ denotes the power spectrum of the input. There are other ways of deriving equation (26), and the reader is referred to references 9, 10, 17, and 18 for a more complete discussion. The important point, however, is that when the input spectrum in equation (26) contains a notch at some frequency, ω_r, the denominator on the right side becomes very small at $\omega = \omega_r$, depending on the notch depth. Therefore, $|H^*(\omega_r)|$ must become correspondingly large. Vice versa, when the input spectrum contains a sinusoid at some frequency, ω_0, the denominator on the right side becomes very large at $\omega = \omega_0$ and $H^*(\omega_0)$ must approach one. It is interesting to note that, with respect to the peak value of $|H^*(\omega)|$ at $\omega = \omega_r$ or ω_0, a prediction filter can respond much more strongly to notches than to signals. It should also be noted that although the "whitening" filter argument only applies when $\Delta = 1$, it does provide an indication of the behavior of $|H^*(\omega)|$ near the notch frequency, even when $\Delta > 1$. (Indeed, as is seen in equation (24), the parameter Δ enters into the expression for $|H^*(\omega)|$ only through the scaling factor, $e^{-\beta\Delta}$, which drives the frequency response to zero as $\Delta \rightarrow \infty$.)

To appreciate more fully the implications of the above results as applied to the ALICE processor, it is important to derive the ALICE output power spectral density $S_y(\omega)$. For the case of negligible ALE weight vector noise, i.e., $\mu_{ALE} \sim 0$, $S_y(\omega)$ is obtained to a good approximation from

$$S_y(\omega) = |H^*(\omega)|^2 \, S_q(\omega). \tag{27}$$

Since we are only interested in the behavior of $S_y(\omega)$ in the vicinity of $\omega = \omega_r$, equation (27) may be approximated by

$$S_y(\omega) \approx |H^*(\omega)|^2 \, S_q^c(\omega), \tag{28}$$

where $|H^*(\omega)|^2$ is computed from equation (24). By substituting equations (15) and (24) into equation (28):

$$S_y(\omega) \approx \frac{\beta^2}{2} \; \frac{\sigma_0^2 \, e^{-2\beta\Delta}}{1 + (\beta^2/2) - \cos(\omega_r - \omega)} \; \chi_L(\omega_r - \omega), \tag{29}$$

where

$$\chi_L(u) = \begin{cases} \sin^2 \dfrac{uL}{2} + \dfrac{(L \cos uL/2 \, \sin u/2 - \sin uL/2 \, \cos u/2)^2}{(L + 2\beta^{-1})^2 \sin^2 u/2} & ; u \neq 0 \\[4mm] 0 & ; \quad u = 0. \end{cases} \tag{30}$$

14

From equations (29) and (30) it is seen that $S_y(\omega)$ can be expressed as a product of the envelope function,

$$F_\beta(\omega_r - \omega) = \frac{\beta^2}{2} \frac{\sigma_0^2 e^{-2\beta\Delta}}{1 + (\beta^2/2) - \cos(\omega_r - \omega)} .$$ (31)

and the oscillatory function, $\chi_L(\omega_r - \omega)$.

A plot of $F_\beta(u)$ and $\chi_L(u)$ is in figure 8. Based on data from figure 8 and equation (31), the shape of the envelope function, $F_\beta(u)$, is seen to resemble closely that of the power spectrum of a finite bandwidth signal whose bandwidth is proportional to β. The peak of $F_\beta(u)$ at $u = 0$ is given by
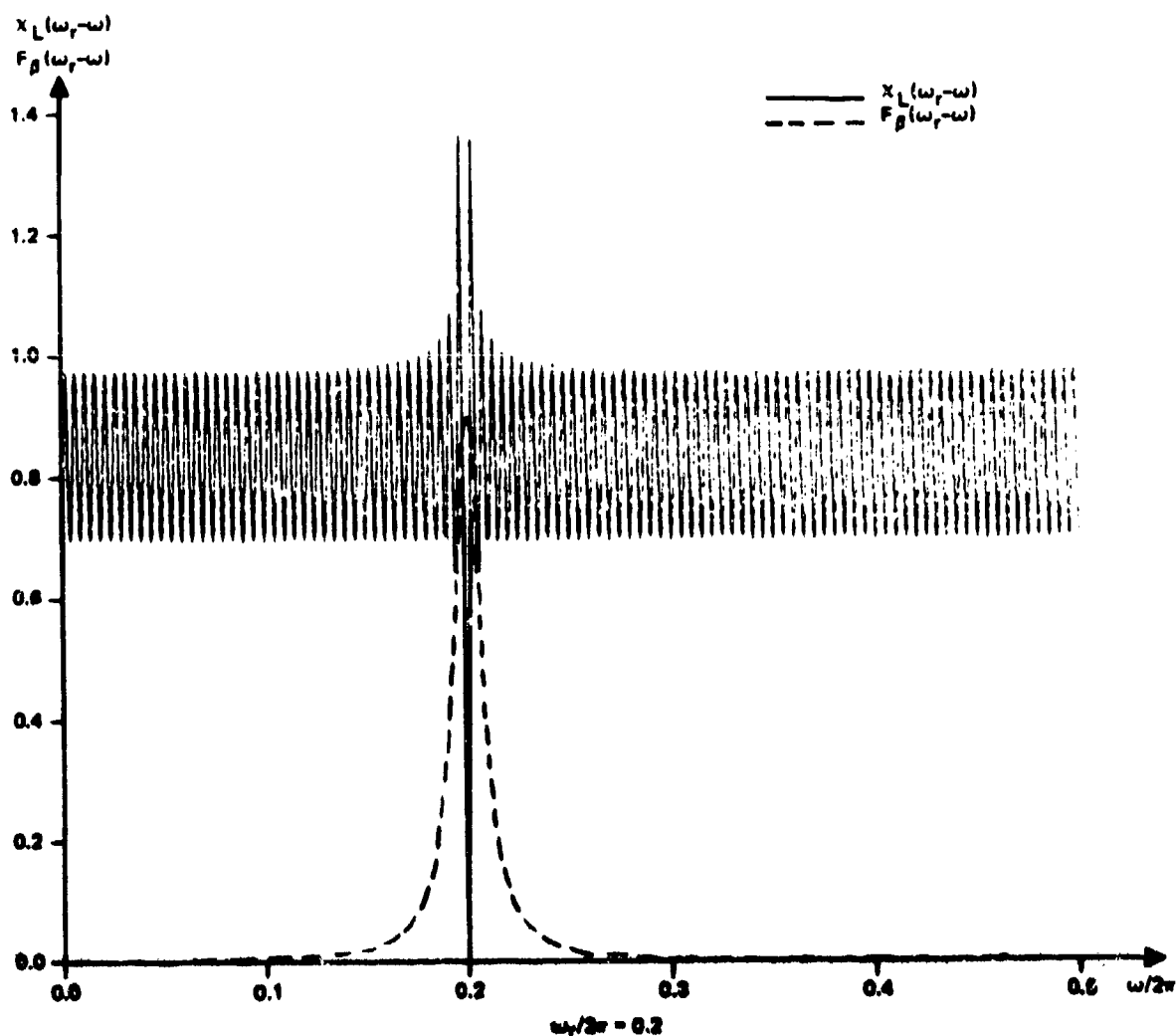
Figure 8. Plot of the envelope function, $F_\beta(\omega_r - \omega)$, and the oscillatory function, $\chi_L(\omega_r - \omega)$. $\beta = 0.05$, $L = 200$, $\sigma_0^2 = 1.0$, and $\Delta = 1$.

15

$$F_\beta(0) = \sigma_0^2 e^{-2\beta\Delta} \tag{32}$$

(from equation (31)). Note that the maximum of $F_\beta(u)$ approaches σ_0^2 for small β and Δ. Based on data from figure 8 and equation (30), the oscillatory function, $\tilde{\chi}_L(u)$, is seen to oscillate uniformly for values of u which are outside the interval, $|u| < 2\pi/L$. Inside this interval, $\chi_L(u)$ peaks to a maximum at $u = \pi/L$, which is approximately given by

$$\chi_L(\pi/L) \approx 1 + 4/\pi^2 \approx 1.4 \tag{33}$$

for $L \gg 2\beta^{-1}$. It then drops to zero at $u = 0$. From equation (30) it is seen that $\chi_L(u)$ converges pointwise to the following limiting function for large L:

$$\chi_L(u) \quad \xrightarrow{L \gg 2\beta^{-1}} \quad \begin{cases} 1 & : \quad u \neq 0 \\ \\ 0 & : \quad u = 0. \end{cases} \tag{34}$$

A plot of the product of F_β and χ_L, i.e., $S_y(\omega)$, is in figure 9. It follows from equations (29) and (34) that, in the limit of large L, $S_y(\omega)$ converges pointwise to the envelope function, i.e.,
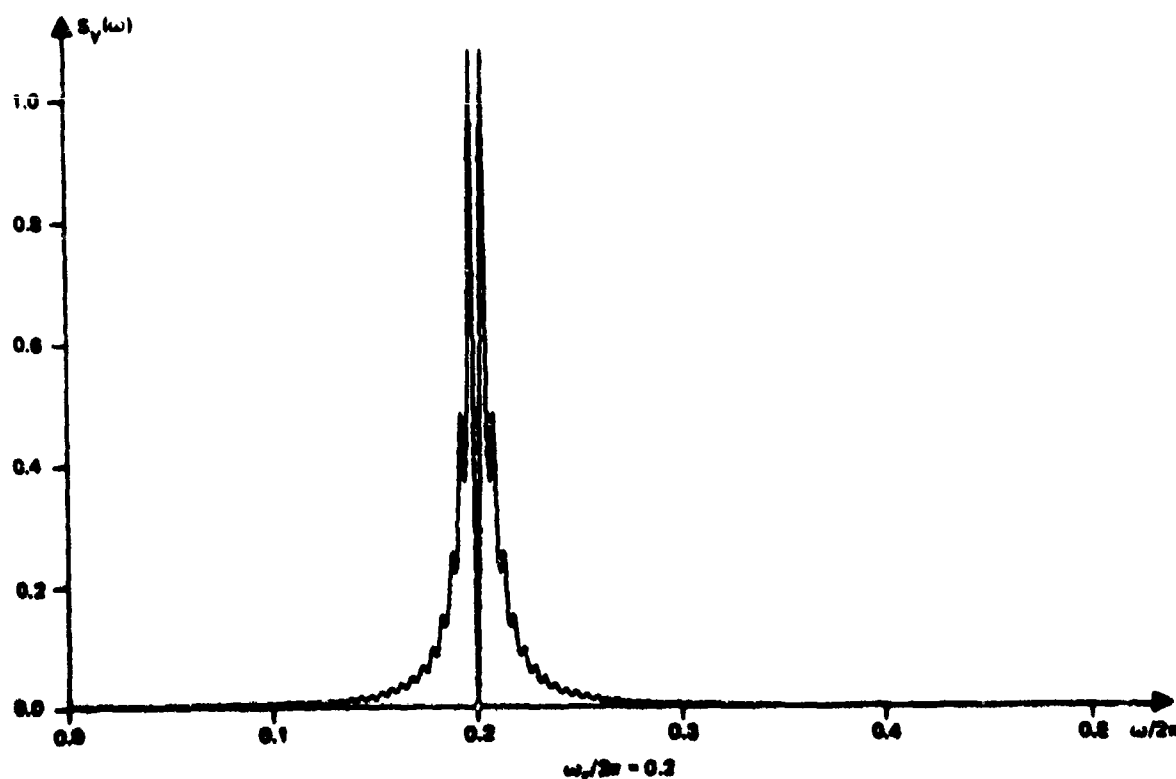
Figure 9. Theoretical plot of the output power spectrum, $S_y(\omega)$. $\beta = 0.05$, $L = 200$, $\sigma_0^2 = 1.0$, and $\Delta = 1.0$.

16

$$S_y(\omega) \xrightarrow{\quad L \gg 2\beta^{-1} \quad} \begin{cases} F_\beta(\omega_r - \omega) \; ; & \omega \neq \omega_r \\[2mm] 0 \; ; & \omega = \omega_r \end{cases} \tag{35}$$

In the vicinity of $\omega = \omega_r$, $S_y(\omega)$ peaks to a maximum which is approximately given by

$$S_y(\omega_r \pm \pi/L) \approx 1.4\, \sigma_0^2\, e^{-2\beta\Delta} \tag{36}$$

(from equations (32) and (33)). Therefore, if the effects of weight vector noise are neglected, the ALE and ALICE output power spectra will closely resemble those of a finite bandwidth signal, when the input to the ALE has a notched, flat power spectrum. However, there is an exception in the vicinity of $\omega = \omega_r$, where $S_y(\omega)$ peaks to a maximum at $|\omega - \omega_r| = \pi/L$ (given approximately by equation (36)) and then drops to zero at $\omega = \omega_r$. This behavior is also evident in figure 9.

TECHNIQUES TO ELIMINATE PEAK IN ALICE OUTPUT SPECTRUM

Since the peak in $S_y(\omega)$, which arises from a notch in the input spectrum, can interfere with the detection of signal peaks, it is desirable to examine different techniques for its elimination. Perhaps the easiest way to remove the peak near $\omega = \omega_r$ is to increase Δ. As seen from equation (29), the peak approaches zero as $e^{-2\beta\Delta}$. Therefore, increasing Δ so that $\Delta \gg \beta^{-1}$ will effectively eliminate it. This is indicated in figure 10A, where a family of curves for $S_y(\omega)$ is plotted for increasing values of Δ. It should be noted that increasing the ALE delay may also decorrelate narrowband signals whose inverse bandwidths are much smaller than Δ.

Another way to eliminate the peak at $\omega = \omega_r$ is to vary β, which is related to the ANC parameters and the power in the reference sinusoid through equation (4). In particular, if $\beta \ll 1/L$, the envelope function $F_\beta(u)$ in equation (31) is so narrow that the product of $F_\beta(u)$ and $\chi_L(u)$ is approximately zero. (This result is reasonable, since, as β approaches zero, the input to the ALE becomes uncorrelated and the right side of equation (13) approaches zero.) Conversely, as β is increased so that $e^{-2\beta\Delta} \ll 1$, the peak of the envelope function approaches zero (from equation (32)) and the peak in $S_y(\omega)$ near $\omega = \omega_r$ is eliminated. The effects of varying β on $S_y(\omega)$ are indicated in figure 10B, where a family of curves for $S_y(\omega)$ is plotted for increasing β.

The addition of uncorrelated noise of power σ_A^2 to the ALE input, suggested by Treichler in reference 19, may also be another way of effectively reducing the peak. The ALE input power spectral density near $\omega = \omega_r$ is approximately given by $S_\eta^c(\omega) + \sigma_A^2$, where $S_\eta^c(\omega)$ is given by equation (15). Note that the effect of σ_A^2 is to reduce the notch depth. Therefore, from the "whitening" filter argument presented earlier, it is expected that the peak in $S_y(\omega)$ near $\omega = \omega_r$ will be reduced. Plots of $S_y(\omega)$ are presented in figure 11 for increasing values of σ_A^2/σ_0^2. As noted in reference 19, it is more effective to modify the ALE's adaptive algorithm, rather than to add noise to the ALE input. Such a modification, which has the same effect as adding noise to the ALE input, has been developed by Treichler (reference 3), and is called the "leaky LMS" algorithm. It should be noted that the disadvantage of adding noise to the ALE input is that the ALE input signal-to-noise ratio of low level signals will be further reduced.

17

A final technique is to examine $Q(\omega) \equiv |1 - H^*(\omega)|^{-2}$ (with $\Delta = 1$). This quantity, which has been referred to by Griffiths in references 9 and 10 as the modified, maximum entropy spectral estimate, gives sharp peaks at the signal frequencies. Furthermore, as can be seen from equation (26), if the input spectrum contains a notch, $Q(\omega)$ in the limit of large L will also contain a notch. This is seen in figure 12, where $Q(\omega)$ is plotted corresponding to an input spectral density given by equation (15). A possible disadvantage with using $Q(\omega)$ is that the resolution capabilities of $Q(\omega)$ are highly dependent on the input signal-to-noise ratios, and for low ratios the variability in the peak values of $Q(\omega)$ can be quite severe (reference 11). Nevertheless, the use of $Q(\omega)$ in the ALICE processor, as opposed to $S_y(\omega)$, may prove quite useful in certain situations, i.e., for high signal-to-noise ratios, and should be further investigated.
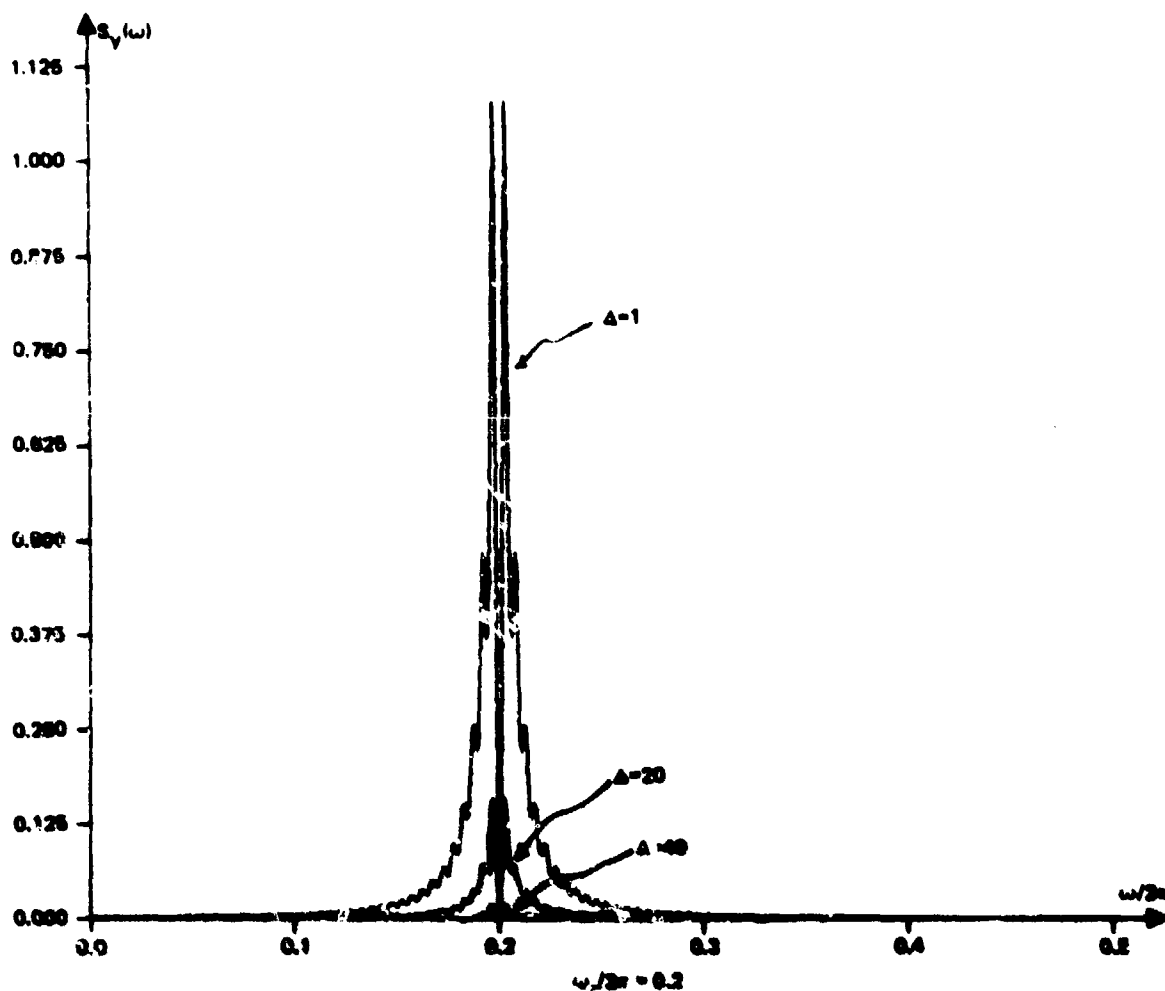
Figure 10. Theoretical plots of the output power spectrum, $S_y(\omega)$. Part A. Values for A. $\beta = 0.5$; $L = 20$; and $\sigma_0^2 = 1.0$.
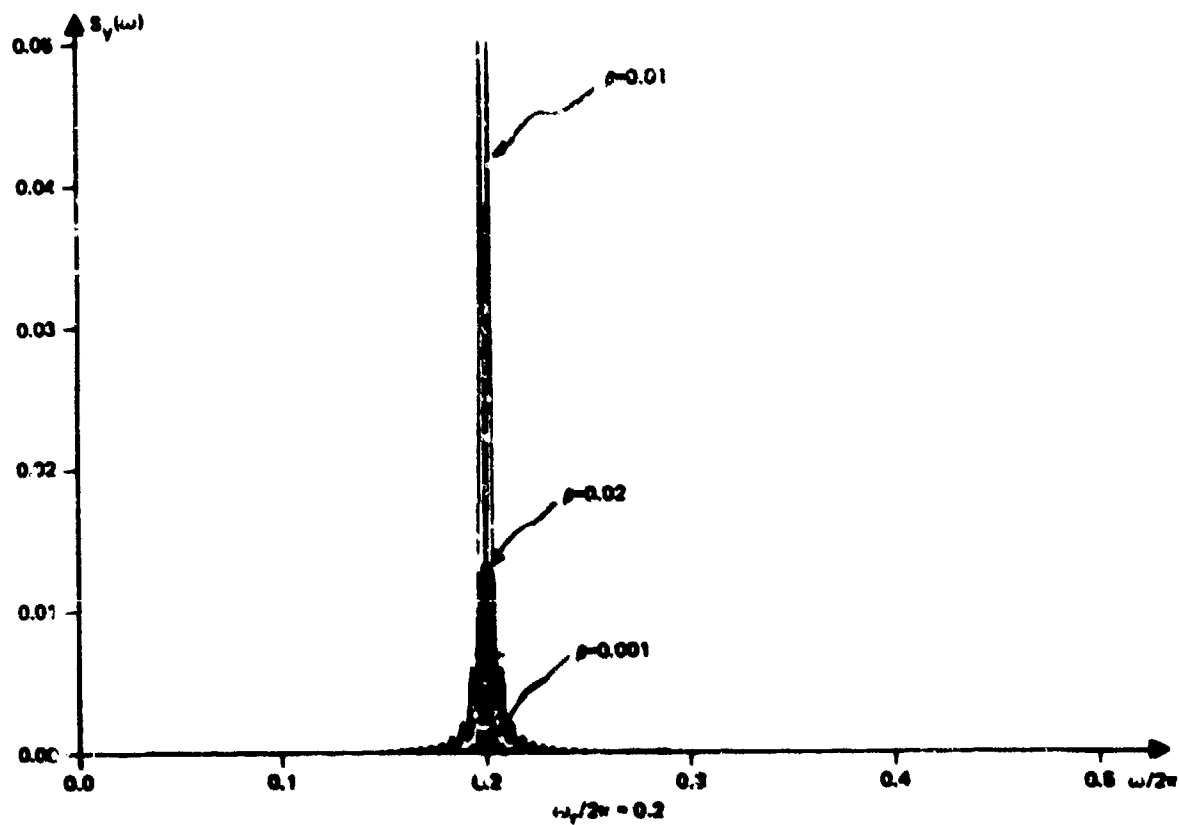
Part B. Values for β. $L = 200$; $\sigma_0^2 = 1.0$; and $\Delta = 100$.
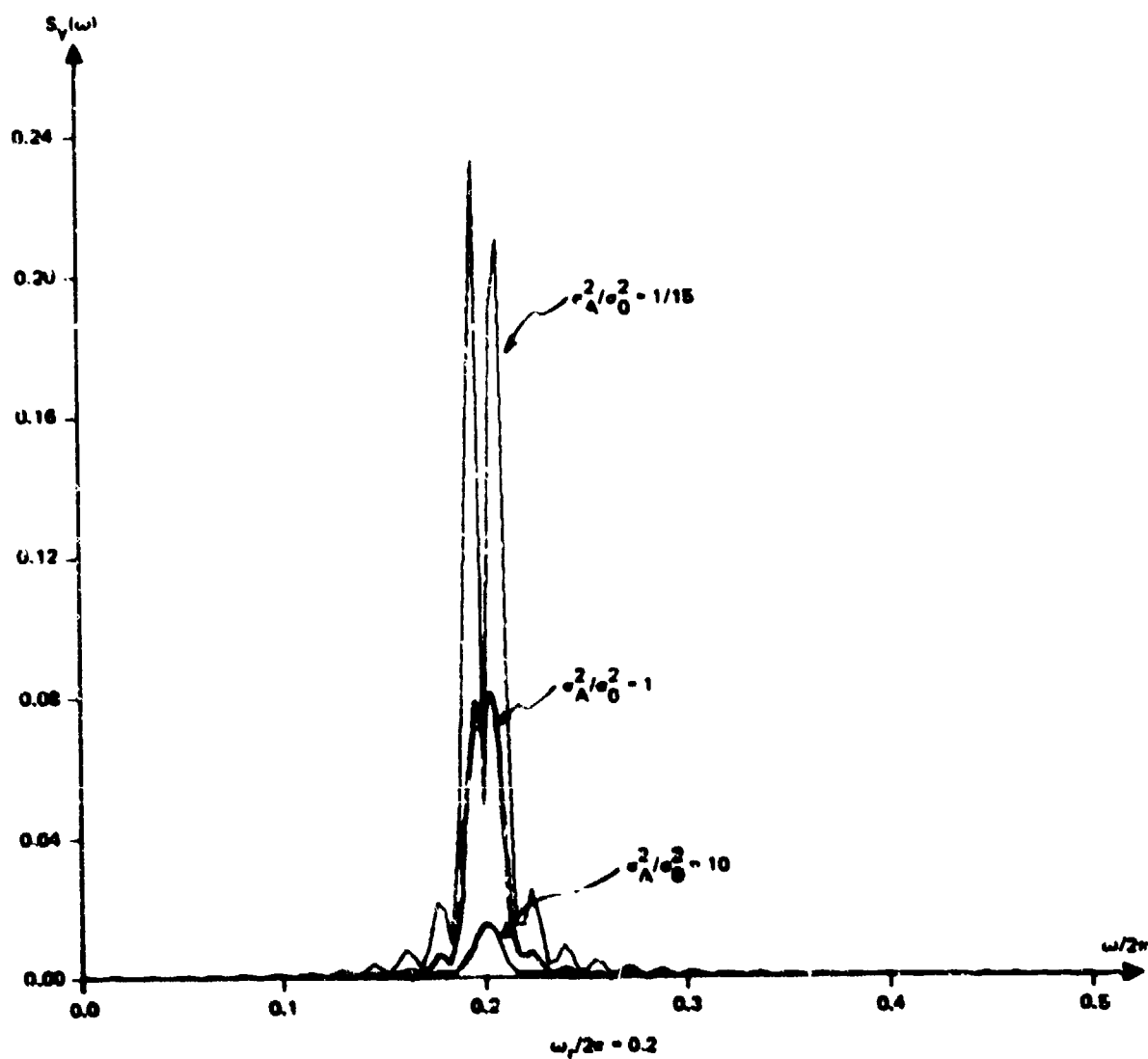
Figure 11. Theoretical plot of the output power spectrum, $S_y(\omega)$, for different values of the ratio, σ_A^2/σ_0^2. $\beta = 0.025$; $L = 64$; $\Delta = 1$; and $\sigma_0^2 = 1.0$.
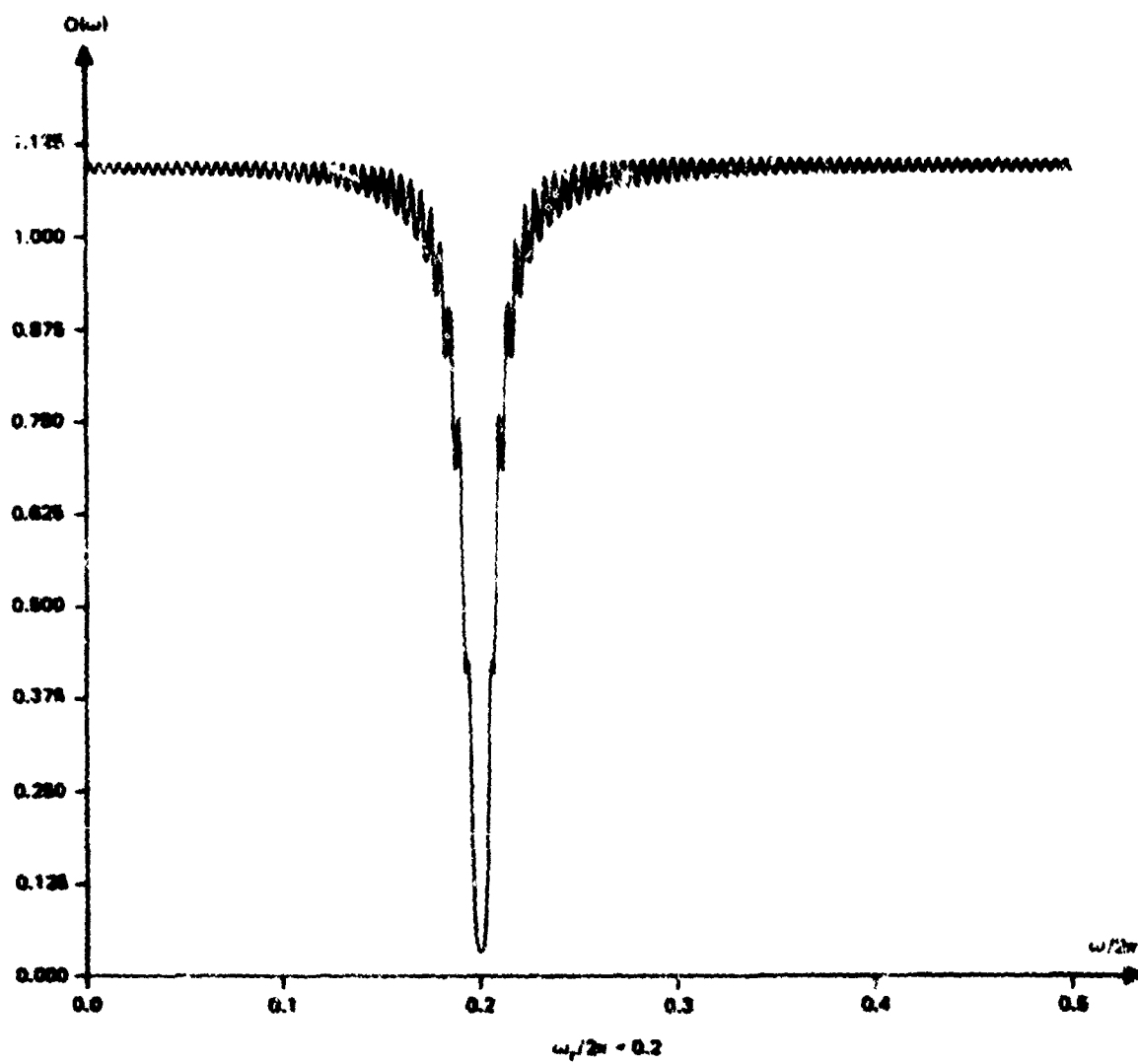
Figure 12. Theoretical plot of the modified, maximum entropy estimate, $Q(\omega)$. $\beta = 0.05$; $\sigma_0^2 = 1.0$; and $L = 200$.

WEIGHT VECTOR NOISE AND TRANSIENT EFFECTS IN ALE RESPONSE TO NOTCHED, INPUT SPECTRUM

In this section, we will consider two factors inherent in the LMS algorithm that strongly affect the ALE's output power spectrum. The first is the level of the background noise spectrum in $S_y(\omega)$, which mainly arises from ALE weight vector noise. The second is the ALE transient response time to a notch. If this time is very long, the peak values for $S_y(\omega)$ (pages 8 through 17) will never be observed, since the ALE will not reach its steady-state behavior. In this section both factors will be examined separately.

Background Noise Level in ALE Output Spectrum

To determine the effects of weight vector noise on the ALE's output, we will derive an expression for the power spectrum of the output, $S_y(\omega)$, which will include the weight vector noise. To do this, the autocorrelation function of the ALICE output, $y(j)$, will be considered first (in correspondence with the treatment in reference 20). The expression for the ALE (ALICE) output, $y(j)$, in terms of the ALE input, $q(j)$, is given by

$$y(j) = \sum_{k=0}^{L-1} (v_k(j) + w_k^*) q(j - k - \Delta) . \tag{37}$$

In equation (37), $v_k(j)$ is the difference between the instantaneous values of the weights determined from equation (11) and the Wiener solution, i.e.,

$$v_k(j) \equiv w_k(j) - w_k^* . \tag{38}$$

The quantity $v_k(j)$ represents the ALE weight vector noise. Its statistical properties have been derived in reference 2 and are further discussed in references 20 and 21. For the case of uncorrelated inputs, $v_k(j)$ is a zero-mean noise component with variance given by $\mu_{ALE} \rho(0)$, where $\rho(0)$ is equal to the total ALE input power. Furthermore, it has been shown (reference 2) that, although each noise component, $v_k(j)$, is highly correlated over time, the weight vector noise components are uncorrelated from weight-to-weight, i.e.,

$$E[v_k(j) v_{k+m}(i)] = \mu_{ALE} \rho(0) \delta(i - j) , \tag{39}$$

where $\delta(k)$ represents a Kronecker delta function.

From equations (37), (38), and (39), as well as a few additional assumptions, we can derive some statistical properties of $y(j)$. In particular, the mean of $y(j)$ is obtained from equation (37):

$$E[y(j)] = \sum_{k=0}^{L-1} E[v_k(j) q(j - k - \Delta)] + \sum_{k=0}^{L-1} w_k^* E[q(j - k - \Delta)]. \tag{40}$$

Each sum in equation (40) vanishes, if $q(j)$ is approximately uncorrelated, which is a very good approximation for $\beta \ll 1$ (see equation (17)). In particular, for the case of uncorrelated inputs, it has been shown (reference 2) that $v_k(j)$ is uncorrelated with $q(j)$ and, therefore, the first sum on the right side of equation (40) vanishes since $v_k(j)$ is zero mean. Also, assuming the uncorrelated noise component in the primary is zero mean and that the ANC may be approximated by a linear, time-invariant filter (a good approximation, references 1 and 2), then $q(j)$ is also zero mean and the second sum on the right side of equation (40) vanishes.

The autocorrelation function of $y(j)$, $r_y(\ell)$, may also be obtained from equation (31):

$$r_y(\ell) \equiv E\{y(j)y(j+\ell)\} = \sum_{k=0}^{L-1} \sum_{k'=0}^{L-1} E\left\{ (v_k(j) + w_k^*)(v_{k'}(j+\ell) + w_{k'}^*)(q(j-k-\Delta)) \right.$$

$$\left. q(j+\ell-k'-\Delta) \right\}. \tag{41}$$

Using the previous assumptions as well as equation (39), we have

$$r_y(\ell) = (\mu_{ALE}L\rho(0))\rho(\ell) + \sum_{k=0}^{L-1} \sum_{k'=0}^{L-1} w_k^* w_{k'}^* \rho(\ell+k-k') . \tag{42}$$

The meaning of each term on the right side of equation (42) becomes clearer upon transforming $r_y(\ell)$ to obtain the power spectrum, $S_y(\omega)$:

$$S_y(\omega) = \sum_{\ell=-\infty}^{\infty} r_y(\ell)e^{-j\omega\ell}$$

$$= (\mu_{ALE}L\rho(0)) S_q(\omega) + |H^*(\omega)|^2 S_q(\omega). \tag{43}$$

The second term on the right side of equation (43) is the output power spectrum from an ALE with negligible misadjustment noise. (This term was analyzed on pages 8 through 17.) The first term on the right side of equation (43) is a scaled version of the input power spectrum, $S_q(\omega)$, and arises from the weight vector noise of the ALE adaptive algorithm. A typical plot of $S_y(\omega)$, calculated from equation (43), is presented in figure 13. The peak in $S_y(\omega)$ near $\omega = \omega_r$ is observed in contrast with the background weight vector noise level, S_y^o. The magnitude of this noise level, S_y^o, is approximately given by

$$S_y^o = \mu_{ALE}L\sigma_0^4 . \tag{44}$$

(from equations (10) and (43)).
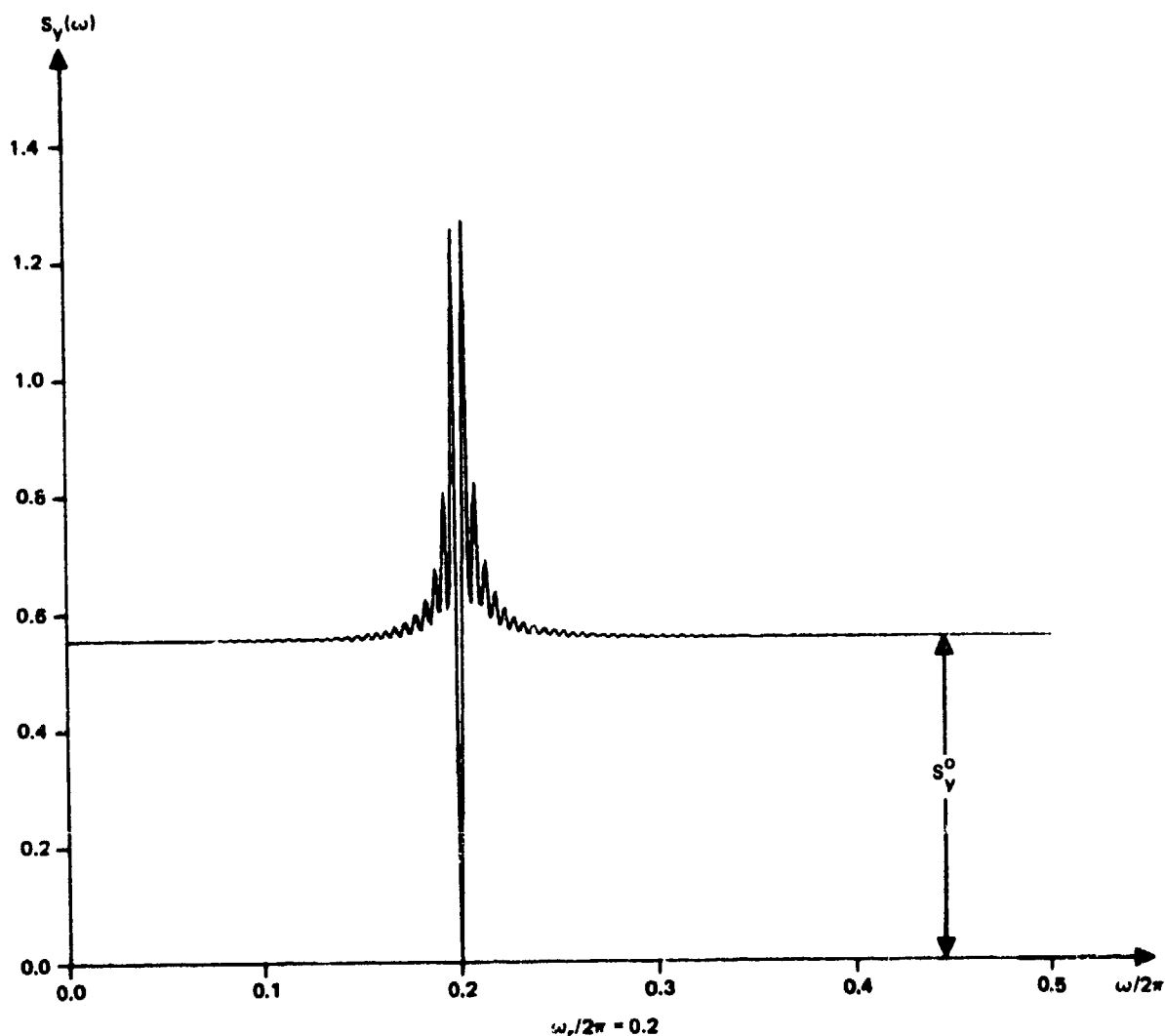
Figure 13. Theoretical plot of the output power spectrum, $S_y(\omega)$, which includes the effects of weight vector noise. $\beta = 0.05$; $L = 200$; $\sigma_0^2 = 1.0$; $\Delta = 1$; and $\mu_{ALE} = 0.0025$.

The determining factor in whether the peak is observed in $S_y(\omega)$ is the ratio R of the peak magnitude to the background noise level, S_y^o. This ratio is approximately given by

$$R \approx 1.4 \cdot e^{-2\beta\Delta}/(\mu_{ALE}\sigma_0^2 L) \tag{45}$$

(from equations (36) and (44)). When $\mu_{ALE}\sigma_0^2 L \ll e^{-2\beta\Delta}$, R becomes quite large and the peak in $S_y(\omega)$ near $\omega = \omega_r$ is clearly observed. Vice versa, for small values of $e^{-2\beta\Delta}$, e.g., $\Delta \gg \beta^{-1}$, R decreases in value and the peak is lost in the background weight vector noise level of $S_y(\omega)$. It is interesting to note that in this latter case $|H^*(\omega)|^2$ approaches zero (as discussed on pages 8 through 17), and that the shape of $S_y(\omega)$ resembles that of the notched input spectrum, $S_q(\omega)$ (see equation (43)).

24

Transient Response Time To a Notch

It has been shown (references 7 and 8) that by diagonalizing the $\underline{R}$ matrix in equation (13) the transients in the mean ALE weight vector will consist of sums of exponentials with time constants given by

$$\tau_p \cong \frac{1}{2\mu_{ALE}\lambda_p} \quad , \tag{46}$$

where λ_p is the pth eigenvalue of $\underline{R}$. In general, a precise treatment of the dynamics of the ALE is very complicated because of difficulties associated with diagonalizing $\underline{R}$. Even for the special case of a notched input power spectrum, given by either equation (10) or equation (15), a closed-form expression for the eigenvalues of the corresponding $\underline{R}$ matrix for arbitrary β, L, and ω_r has not been derived. However, as noted by Treichler (reference 19), when the product βL is much smaller than one, the autocorrelation function of $q(j)$, viz, $\rho(\ell)$, closely resembles that for a sinusoid in white noise (see equation (17)). Therefore, under the assumption that $\beta L \ll 1$, Treichler (reference 19) shows (in correspondence with the analysis in reference 3) that the ALE time constant for a notch is approximately given by

$$\tau_{NOTCH} \simeq \frac{1}{2\mu_{ALE}\,\sigma_0^2}\frac{1}{(1-\beta L/2)} \cdot ,\beta L \ll 1. \tag{47}$$

It is interesting to compare equation (47) with the ALE time constant for a sinusoid with power σ_s^2 in white noise with power σ_0^2:

$$\tau_{SIG} \simeq -\frac{1}{2\mu_{ALE}\,(\sigma_0^2 + \sigma_s^2\,L/2)} \tag{48}$$

(from reference 3). Comparing equations (47) and (48) reveals that, with respect to the ALE convergence time, a notch in white noise may be thought of as a sinusoid with negative power, $-\sigma_0^2\beta$, in the limit of small βL. This, in turn, implies that the ALE response time to notches will generally be longer than the ALE response time to signals. It must be emphasized that these transient results are only valid for $\beta L \ll 1$. A more general treatment of the ALE transient response to notches has not yet been attempted.

EXPERIMENTAL RESULTS

ALE RESPONSE TO A NOTCHED INPUT SPECTRUM

In this section, experimental plots of the steady-state ALE output power spectrum are presented, where the input spectrum consists of a notch in white noise. The input, $q(j)$, is generated by passing white noise into the primary channel of an ANC and passing a sine wave with voltage, V_{ref}, into the reference channel of an ANC (figure 14). The ANC used in these experiments was built at NOSC, whereas the ALE was built at the Autonetics Division of Rockwell. In all experiments, the sample frequency was 2162 Hz.
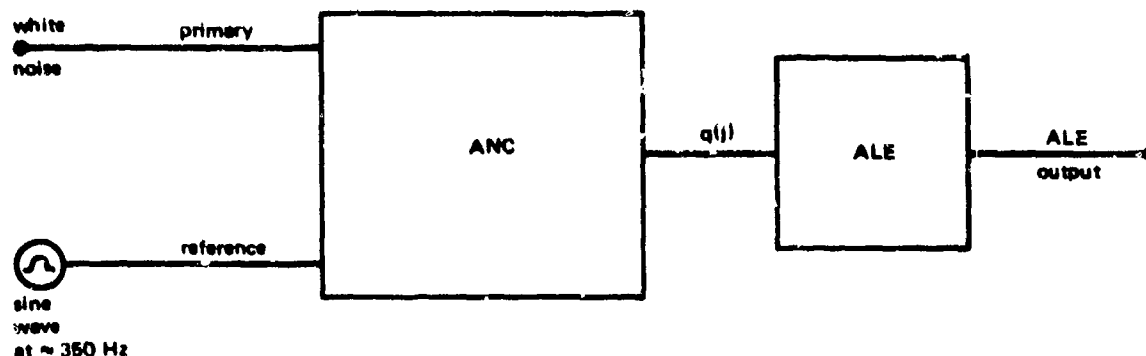
Figure 14. Test setup used to generate ALE output power spectrum. The noise bandwidth was 1 kHz and the noise voltage was 0.6-V rms.

The first set of experiments (figures 15, 16, and 17) was performed to examine the effect of increasing the ALE delay, Δ, on the ALE output power spectrum. As previously discussed such an increase should decorrelate the notch and therefore eliminate the peak $S_y(\omega)$ near the notch frequency (see pages 8 through 17). This is clearly observed in figures 15 through 17, where Δ is increased from 200 to 1000 samples or, equivalently, from 93 to 463 msec. When $\Delta = 200$ samples, the peak in $S_y(\omega)$ is obviously evident (figure 15B). In figure 15D, the fine structure of the peak can be examined in more detail; in particular, a null in the center of the peak is evident. The presence of this null is in agreement with the analytical results obtained on pages 8 through 17. Also, a comparison between the 3-dB width of the peak in figure 15D and the 3-dB notch width in figure 15C reveals good agreement within the noise variances of the spectrum plots. This is also in agreement with the analytical results on pages 8 through 17. When Δ is increased to 350 samples, the peak is flattened (figures 16B and 16D). When $\Delta = 1000$, the notch is completely decorrelated by the ALE, and the ALE output power spectrum also contains a notch (figure 17D). This is in agreement with the discussion on pages 22 through 25.

In figures 18, 19, and 20, the effects of increasing the notch width on the ALE output are examined. As β is increased, the peak in the ALE output power spectrum will eventually decrease (see pages 17 through 21). This is clearly evident in the figures, where the reference voltage is increased. Increasing V_{ref} also increases β (equation (4)). In figure 18, where $V_{ref} = 0.6$-V rms, a large peak in $S_y(\omega)$ is observed at the notch frequency. However, when V_{ref} is further increased to 1.3-V rms (figure 19), the peak is flattened. When V_{ref} is further increased to 1.5-V rms (figure 20), the product, $\beta\Delta$, is large enough so that the ALE has completely decorrelated the notch and a notch now appears in the output power spectrum (in accordance with the discussion on pages 22 through 25).

Part A. ALE input spectrum from 0 to 1 kHz.
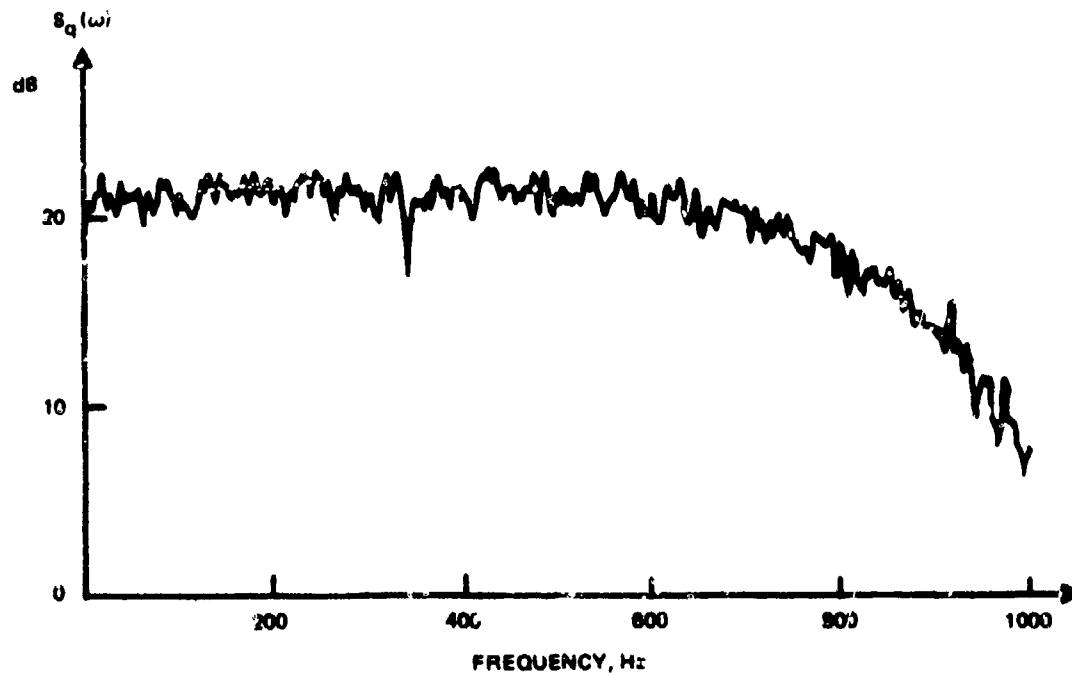
Part B. ALE output spectrum from 0 to 7 kHz.
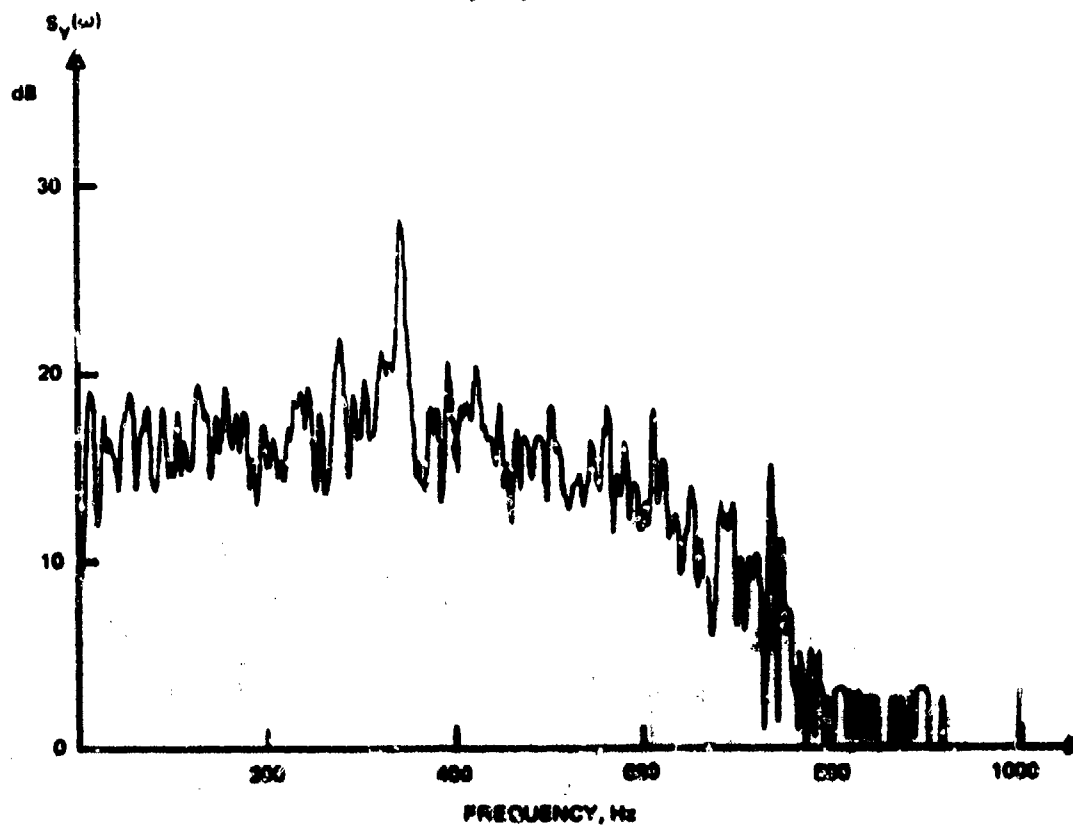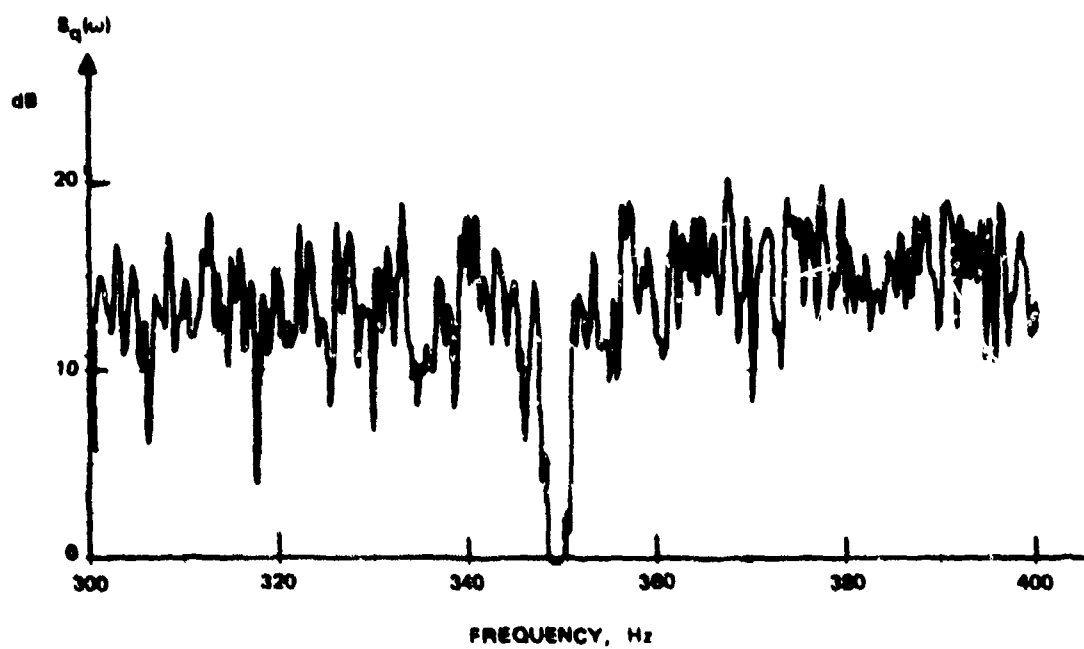

Figure 15. ALE response to a notch for $L = 2046$, $N = 128$, $\mu_{ALE} = 2^{-13}$, $\mu_{ANC} = 2^{-10}$, $\Delta = 200$, and $V_{ref} = 0.88$-V rms.

Part C. ALE input spectrum from 300 to 400 Hz.
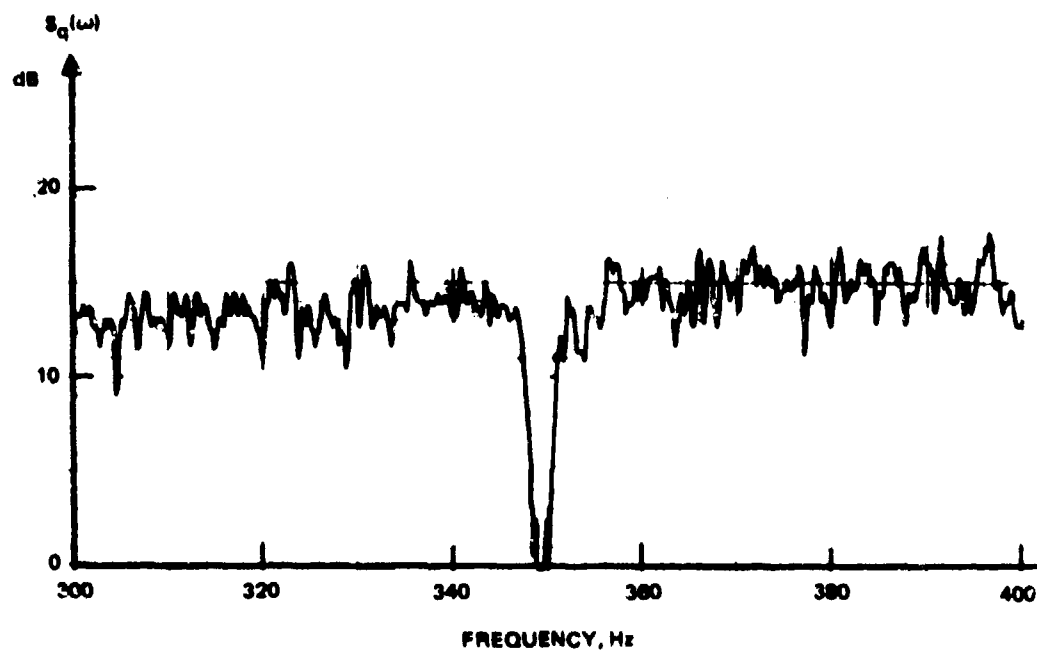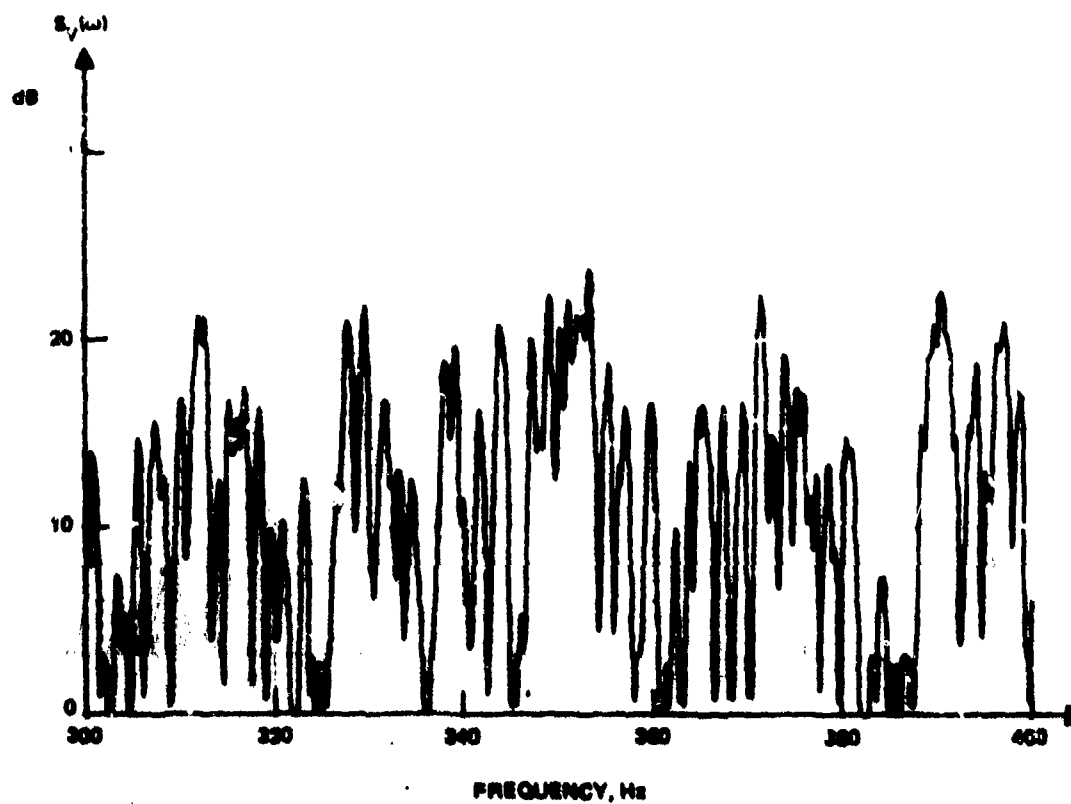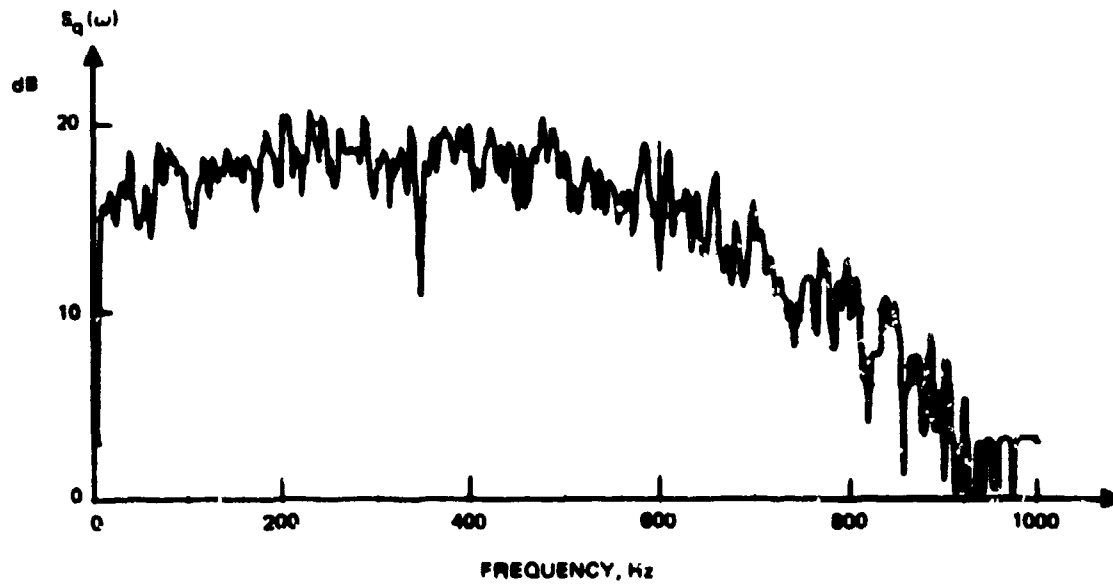

Part D. ALE output spectrum from 300 to 400 Hz.
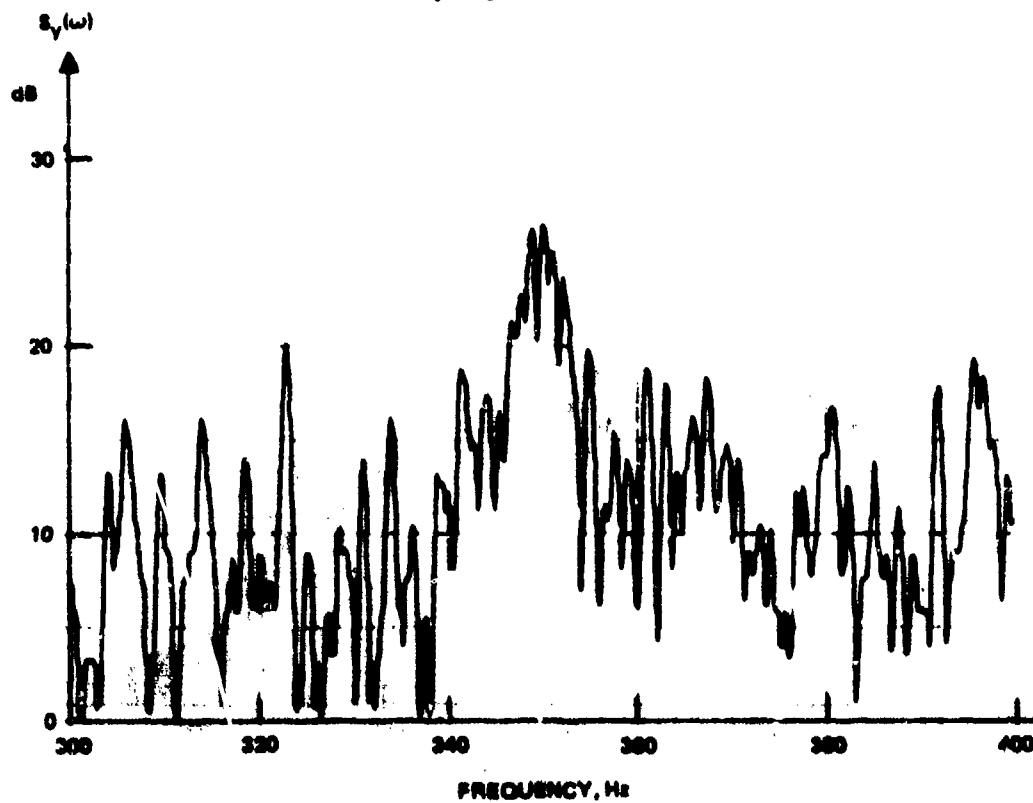
Figure 15. Continued.

28

Part A. ALE input spectrum from 0 to 1 kHz.
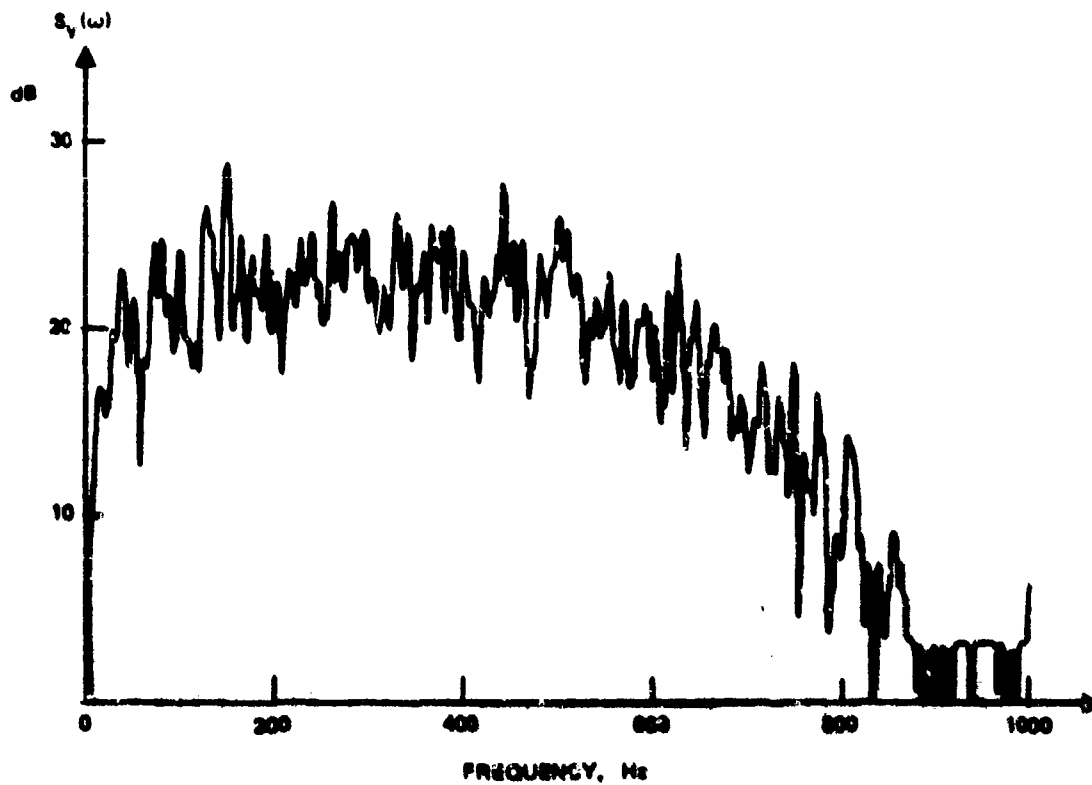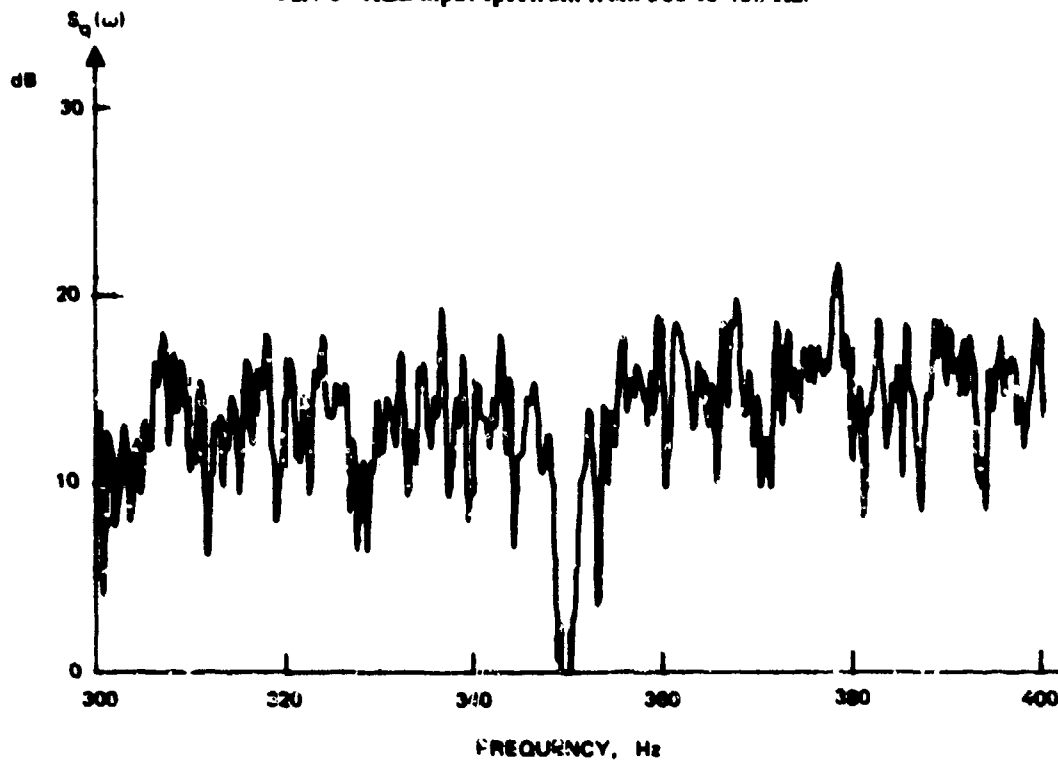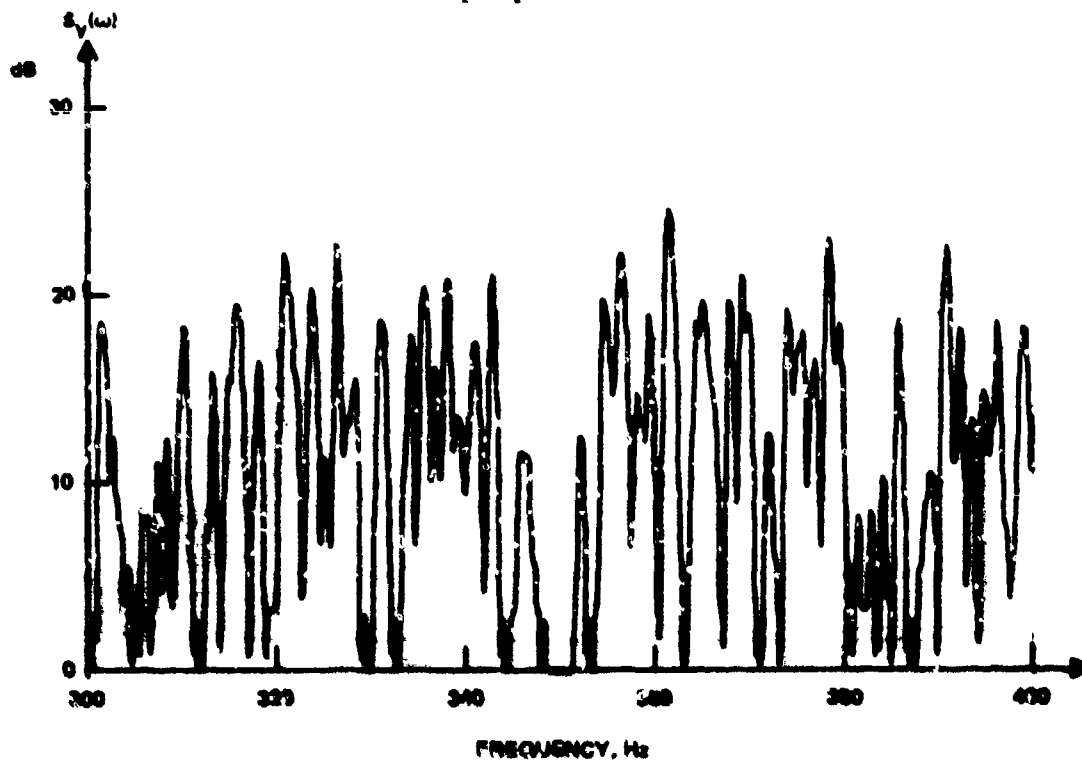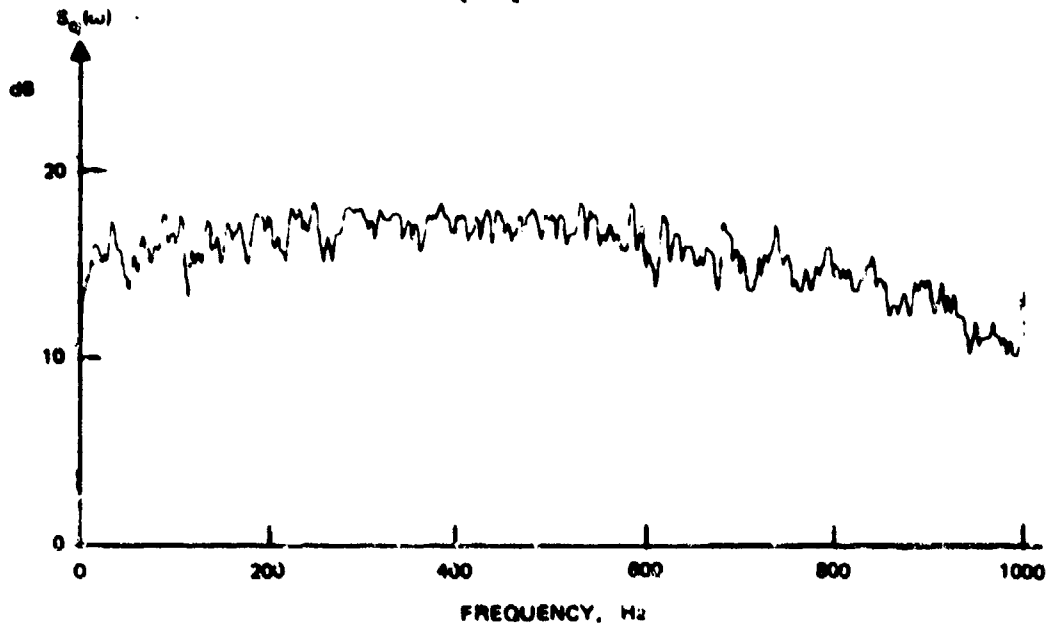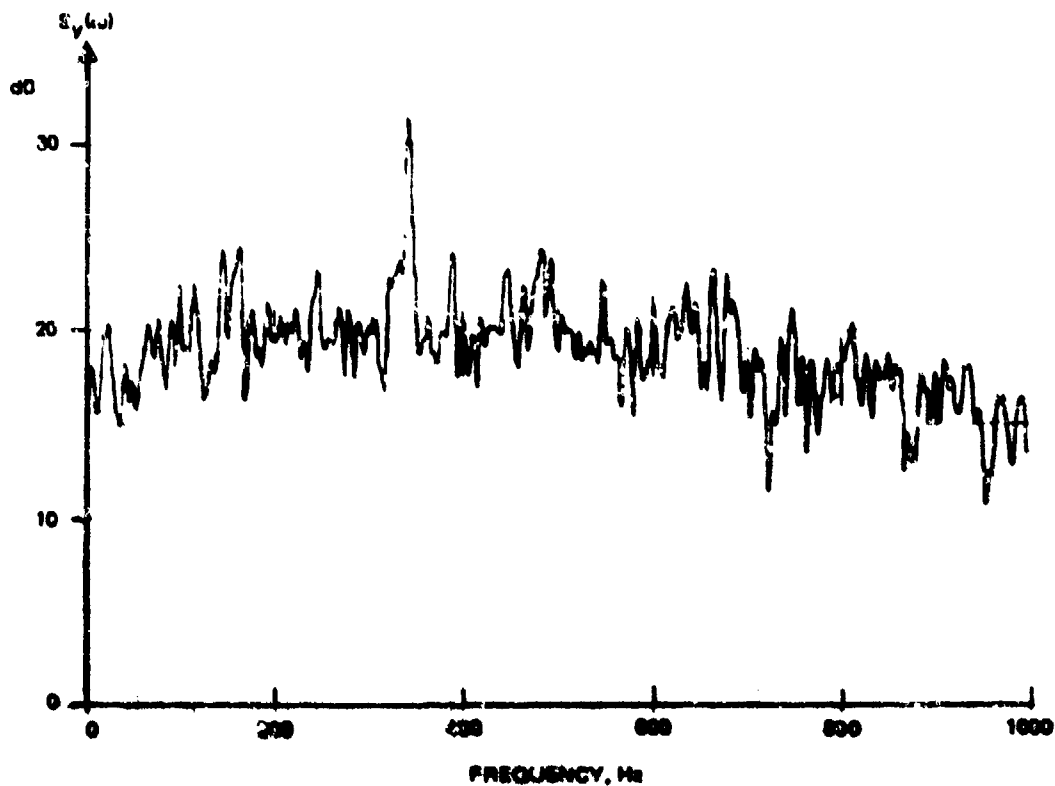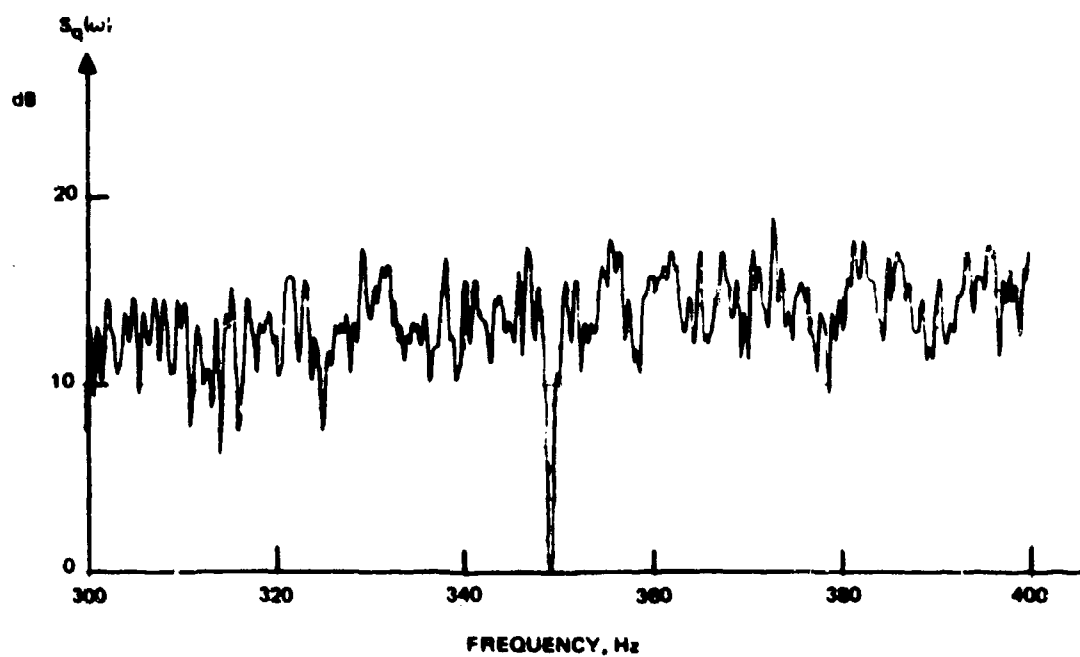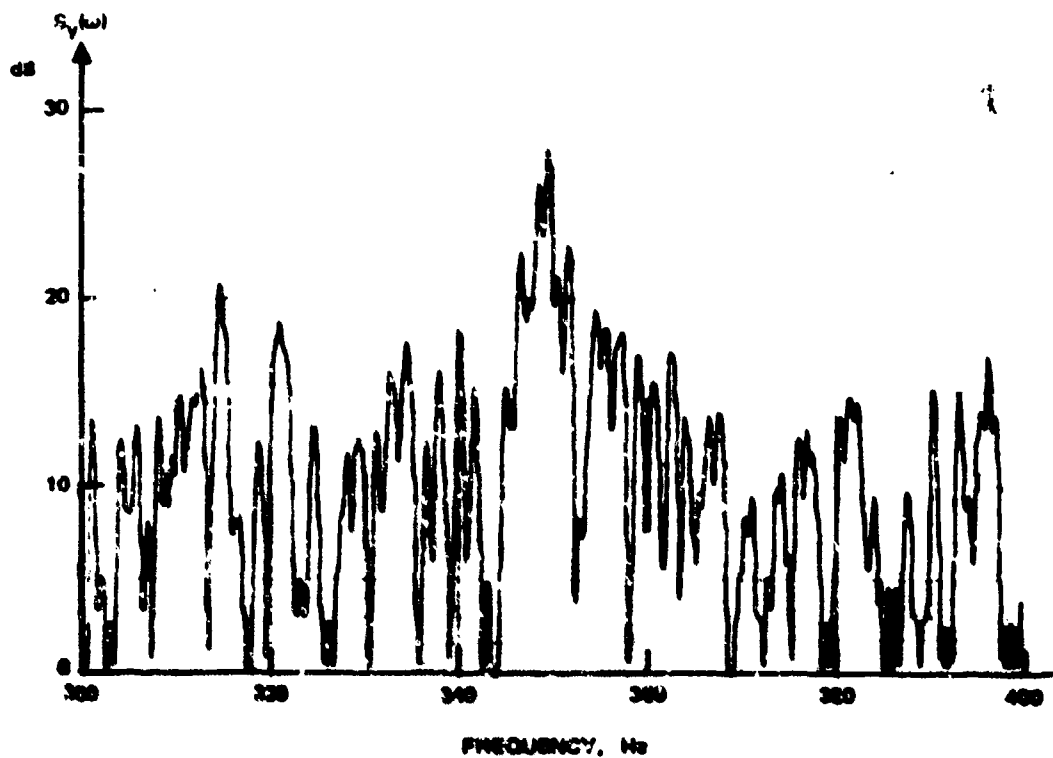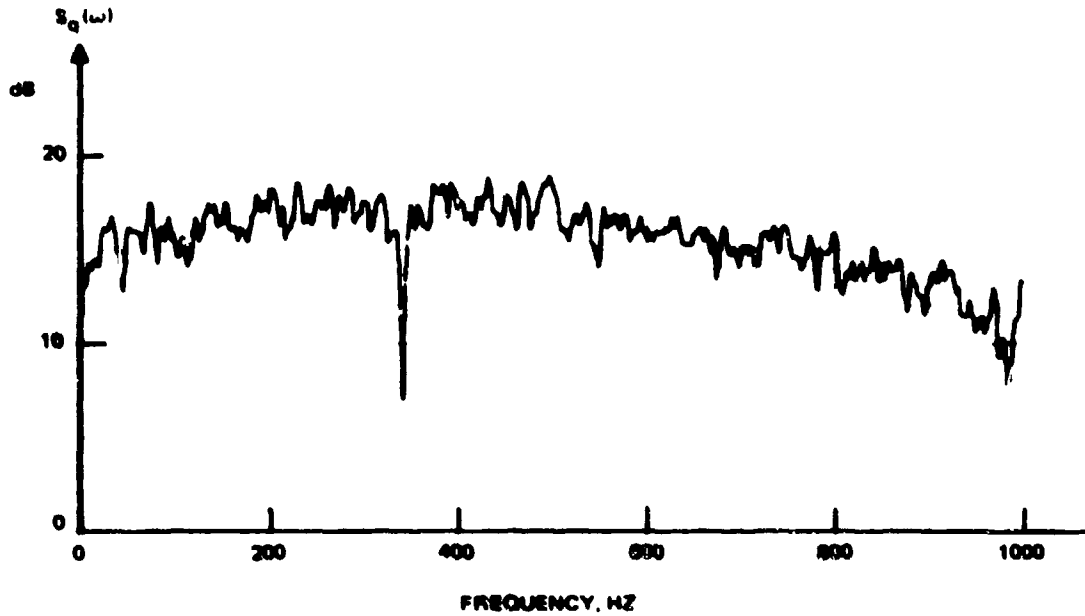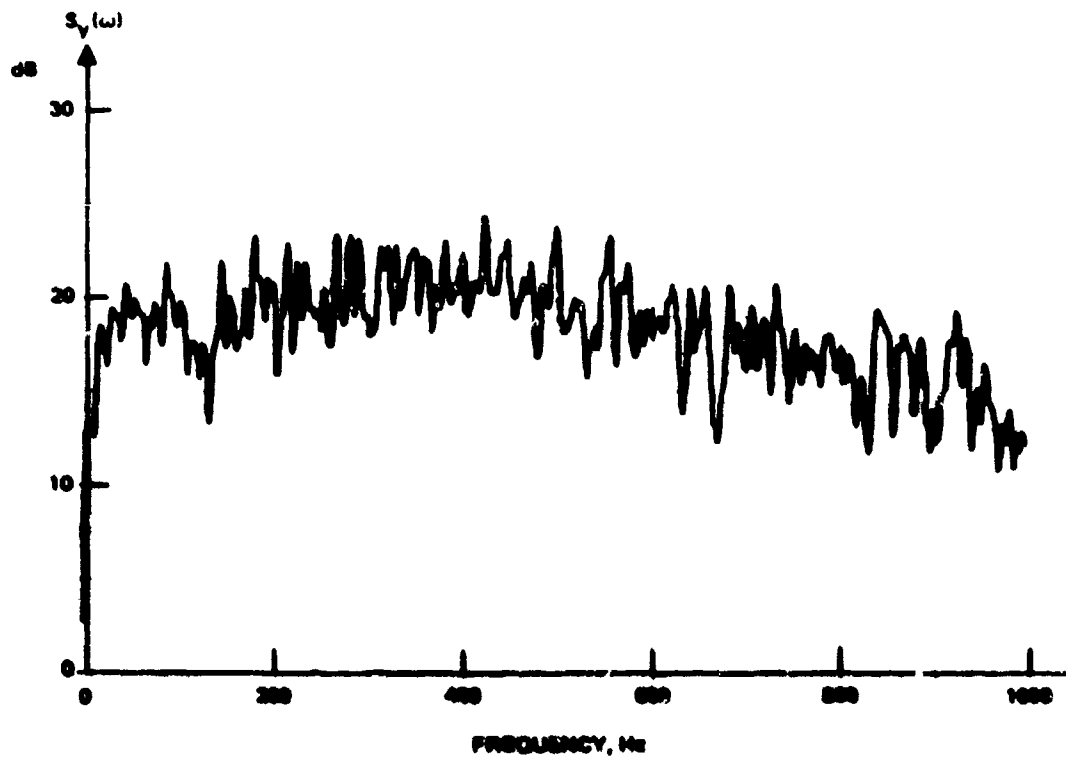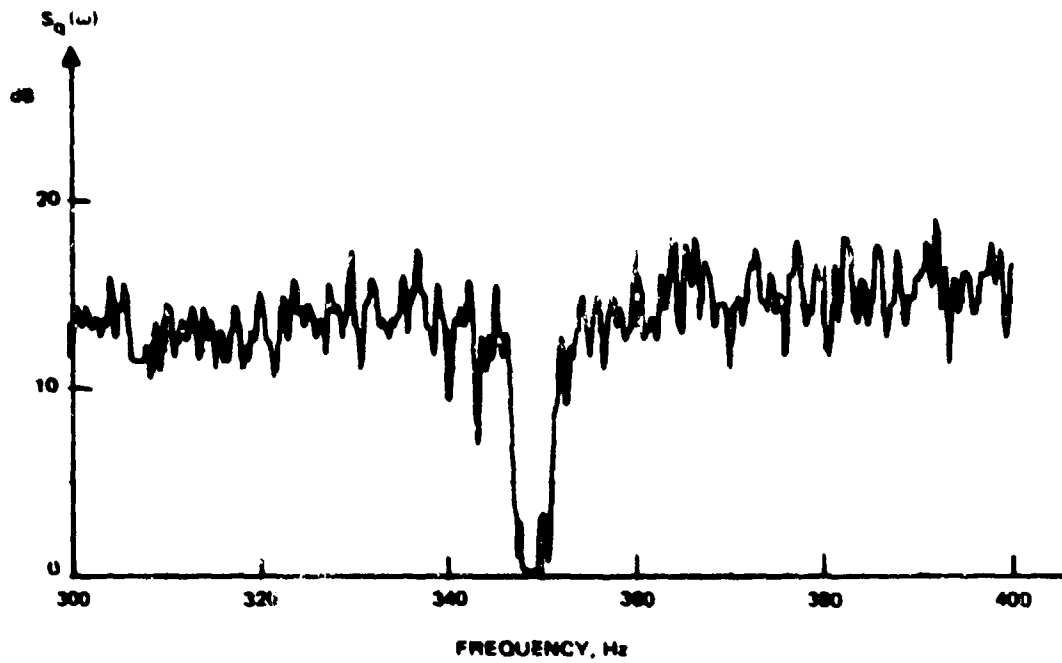

Part B. ALE output spectrum from 0 to 1 kHz.

Figure 16. ALE response to a notch for $L = 2046$, $N = 128$, $\mu_{ALE} = 2^{-13}$, $\mu_{ANC} = 2^{-10}$, $\Delta = 350$, and $V_{ref} = 0.38$-V rms.

Part C. ALE input spectrum from 300 to 400 Hz.

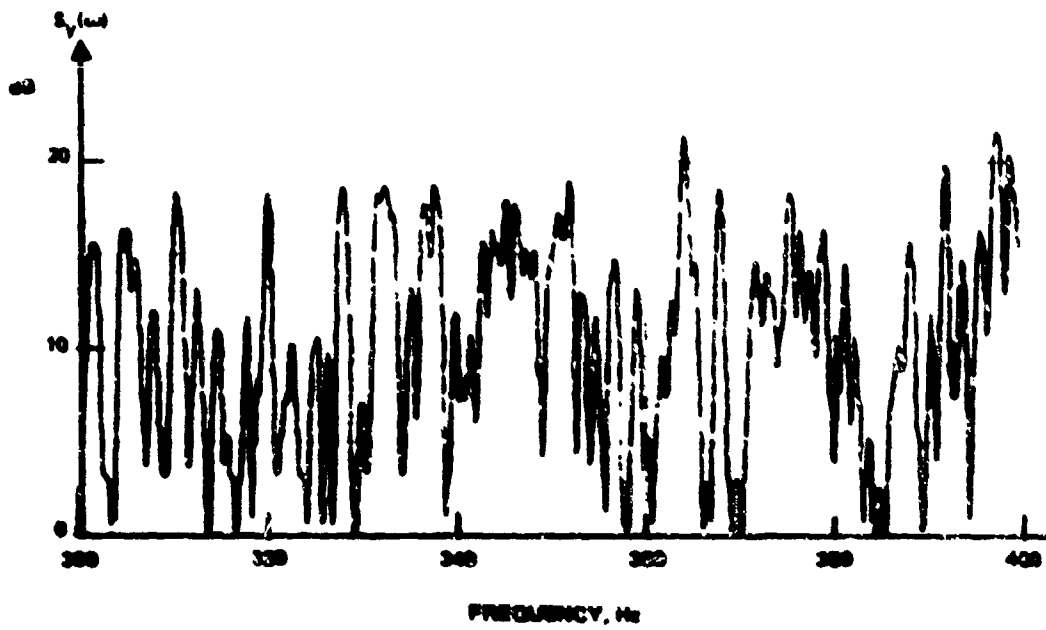Part D. ALE output spectrum from 300 to 400 Hz.

Figure 16. Continued.

Part A. ALE input spectrum from 0 to 1 kHz.

Part B. ALE output spectrum from 0 to 1 kHz.

Figure 17. ALE response to a notch for $L = 2046$, $N = 128$, $\mu_{ALE} = 2^{-13}$, $\mu_{ANC} = 2^{-10}$, $\Delta = 1000$, and $V_{ref} = 0.88$-V rms.

Part C. ALE input spectrum from 300 to 400 Hz.

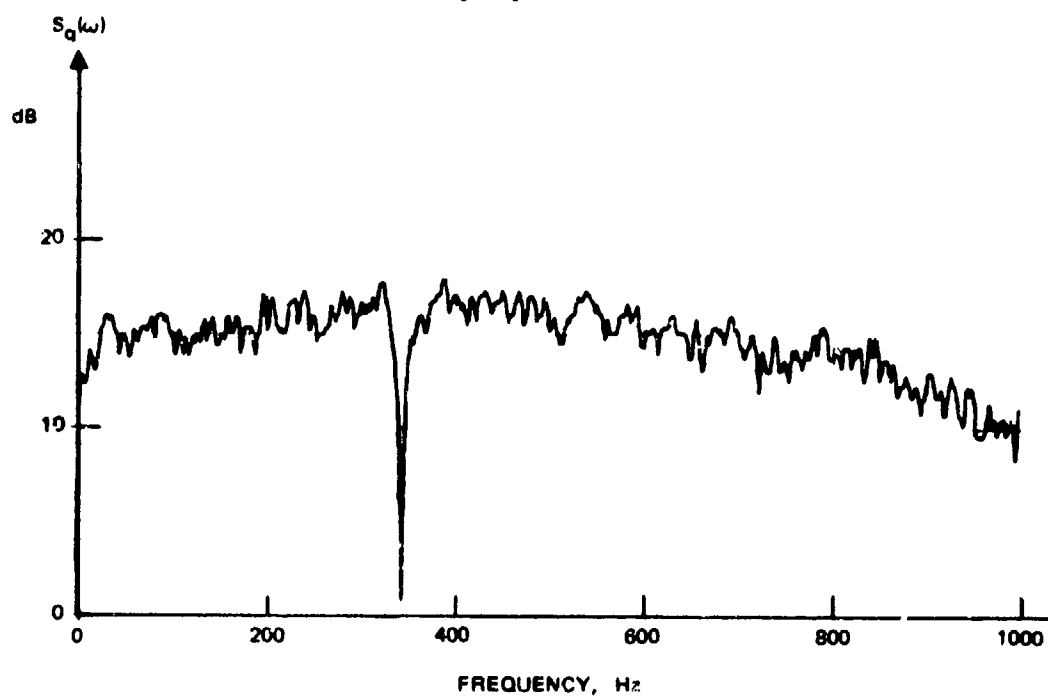Part D. ALE output spectrum from 300 to 400 Hz.

Figure 17. Continued.

32

Part A. ALE input spectrum from 0 to 1 kHz.

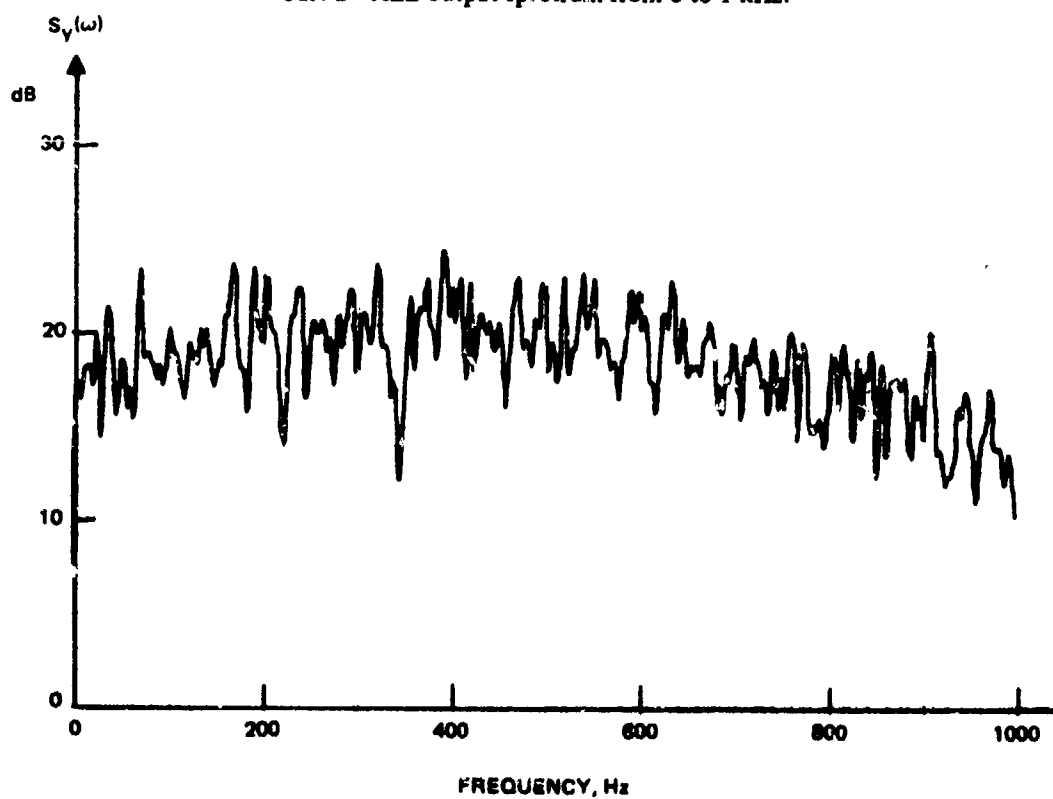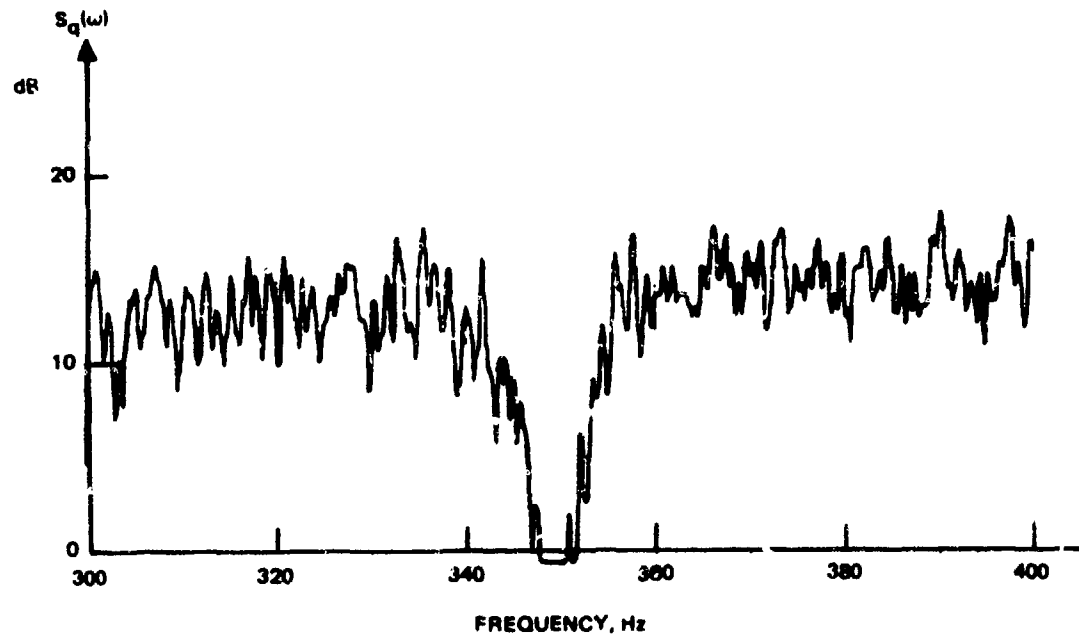Part B. ALE output spectrum from 0 to 1 kHz.

Figure 18. ALE response to a notch for $L = 2046$, $N = 128$, $\mu_{ALE} = 2^{-13}$, $\mu_{ANC} = 2^{-10}$, $\Delta = 200$, and $V_{ref} = 0.6$-V rms.

33

Part C. ALE input spectrum from 300 to 400 Hz.

Part D. ALE output spectrum from 300 to 400 Hz.

Figure 18. Continued.

34

Part A. ALE input spectrum from 0 to 1 kHz.

FREQUENCY, HZ

Part B. ALE output spectrum from 0 to 1 kHz.

FREQUENCY, Hz

Figure 19. ALE response to a notch for $L = 2046$, $N = 128$, $\mu_{ALR} = 2^{-13}$, $\mu_{ANC} = 2^{-10}$, $\Delta = 200$, and $V_{ref} = 1.3$-V rms.

Part C. ALE input spectrom from 300 to 400 Hz.
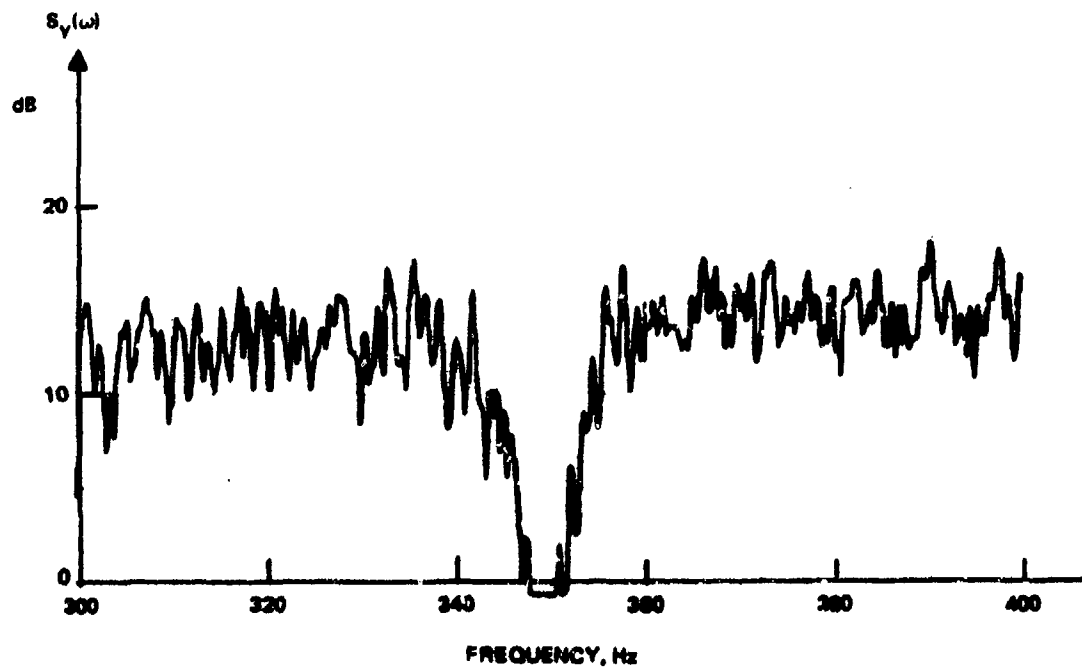

Part D. ALE output spectrum from 300 to 400 Hz.

Figure 19. Continued.

36

Part A. ALE input spectrum from 0 to 1 kHz.

Part B. ALE output spectrum from 0 to 1 kHz.

Figure 20. ALE response to a notch for $L = 2046$, $N = 128$, $\mu_{ALE} = 2^{-13}$, $\mu_{ANC} = 2^{-10}$, $\Delta = 200$, and $V_{ref} = 1.5$-V rms.

Part C. ALE input spectrum from 300 to 400 Hz.

Part D. ALE output spectrum from 300 to 400 Hz.

Figure 20. Continued.

ALICE RESPONSE TO NOTCHES

In this section, results of experiments performed on a hardware implementation of ALICE (designed and built by Rockwell) are presented. This particular device implements both the ANC and ALE in one unit and represents a realistic implementation of ALICE.

The purpose of this section is to establish a range of values for some of the ALICE parameters so that undesirable peaks in the ALICE output, which arise from cancelling sinusoidal interferences, can be eliminated. For these experiments, the inputs to the primary channel of the ALICE consisted of white noise and a sine wave. The noise bandwidth was 1 kHz and the noise voltage was 1-V rms. The frequency of the sinusoid in the primary channel was 200 Hz and the voltage was 0.1-V rms. The inputs to the reference channels were two sinusoids at 200 and 454 Hz. The voltages of the 200- and 454-Hz sinusoids were 0.1-V rms and 0.5-V rms, respectively, and the sample frequency was 2162 Hz. A diagram of the experiment is in figure 21 and a plot of the power spectrum of the primary input is in figure 22. The input to the ALE part of the ALICE processor consisted of two notches at 200 and 454 Hz.

In the first set of experiments (figures 23, 24, and 25), the ALE delay was varied from 200 to 1000. The adaptation parameters were set to $\mu_{ANC} = 2^{-10}$ and $\mu_{ALE} = 2^{-13}$. In addition, N was set equal to 87 and L to 638. The trends of the experiments were similar to those in figures 15, 16, and 17. In figure 23A, a plot of the ALICE output power spectrum is presented 1 minute from the start of adaptation for $\Delta = 200$; there are no large peaks at the notch frequencies. (As noted on pages 22 through 25, the ALE adaptation of time for notches is generally much longer than the ALE adaptation time for signals.) In figure 23B, which was made 5 minutes after the start of adaptation, two peaks at the notch frequency are clearly visible. Even when Δ is increased to 500, two peaks are still evident (figure 24B). However, when Δ is increased to 1000, the peaks at the notch frequencies are gone after 5 minutes of adaptation (figure 25B).

In figures 26, 27, and 28, the widths of both notches in the ALE input spectrum have been increased by increasing μ_{ANC} to 2^{-8} and keeping the values for μ_{ALE}, N, and L the same as in figures 23 through 25. The ALE delay is then once again varied from 200 to 1000 samples. When $\Delta = 200$ samples, peaks at the notch frequencies can be seen after 5 minutes of adaptation (figure 26B). However, when Δ is increased to 500 and 1000, the products of the notch widths and Δ are large enough so that ALICE has completely decorrelated the notches and the notches now appear in the ALICE output after 5 minutes of adaptation (figures 27B and 28B).
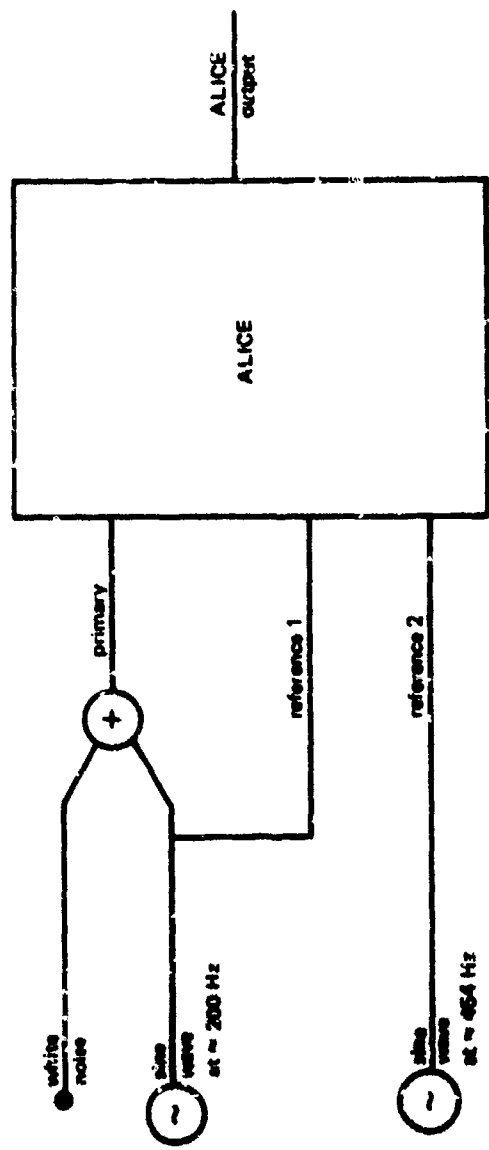
Figure 21. Test setup used to generate range of values for ALICE parameters. The noise bandwidth was 1 kHz and the noise voltage was 1-V rms.
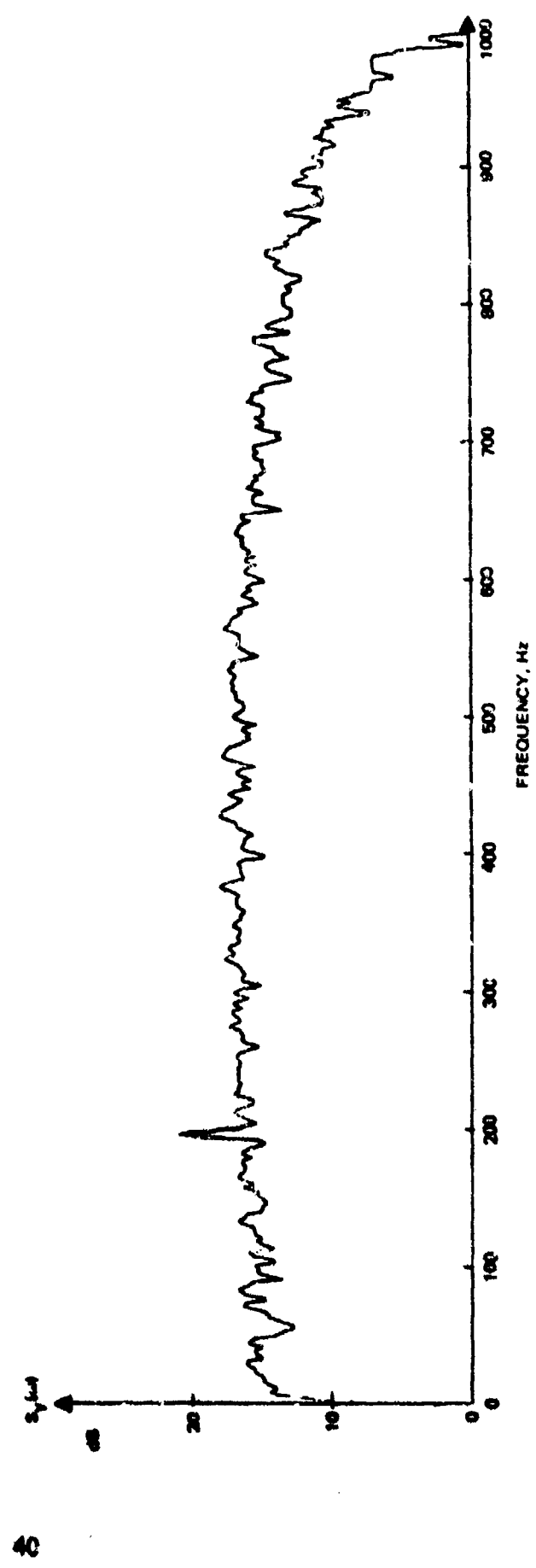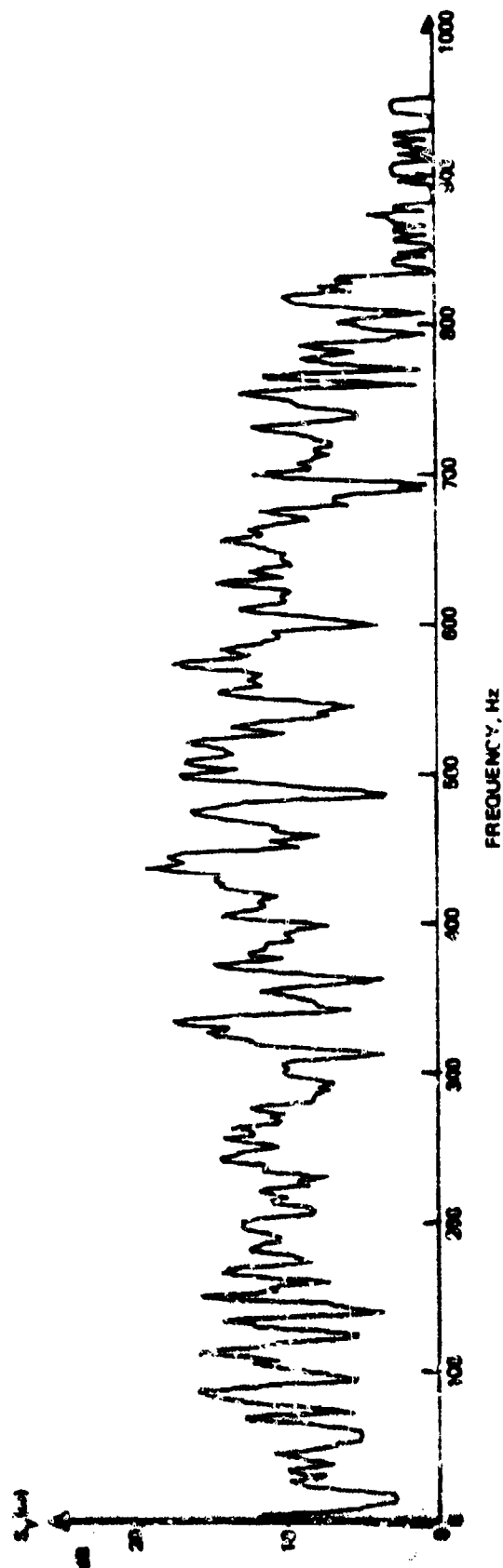

Figure 22. Power spectrum of the primary input to ALICE.

40

Part A. 1 minute after start of adaptation.

FREQUENCY, Hz

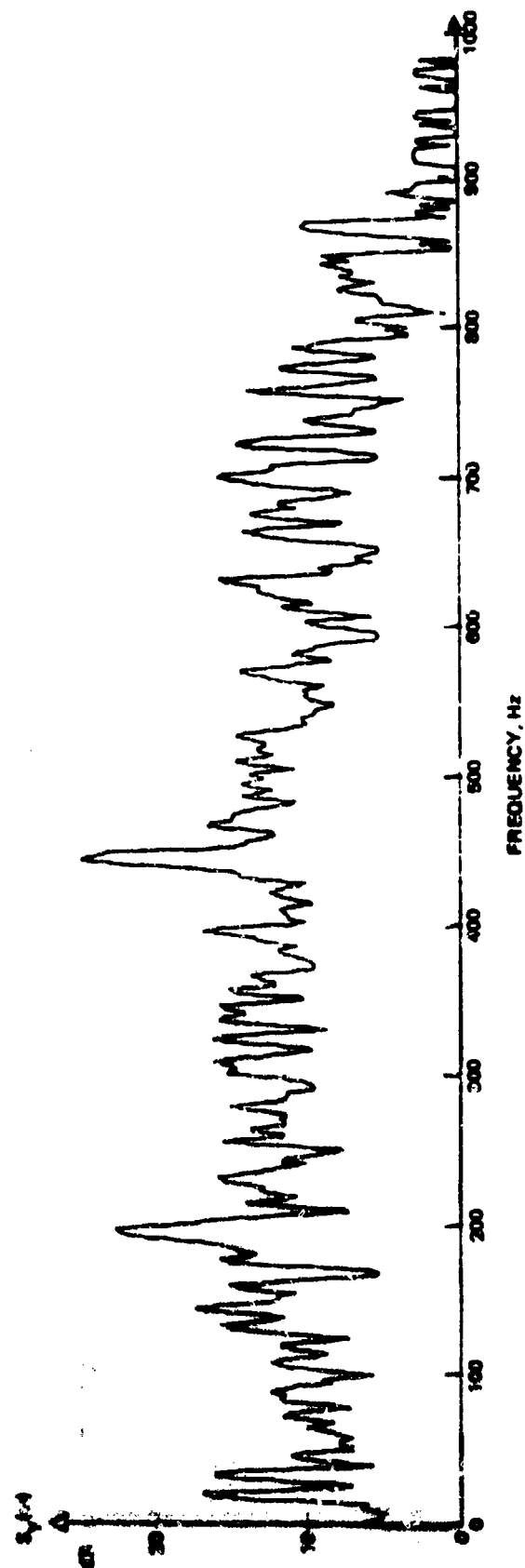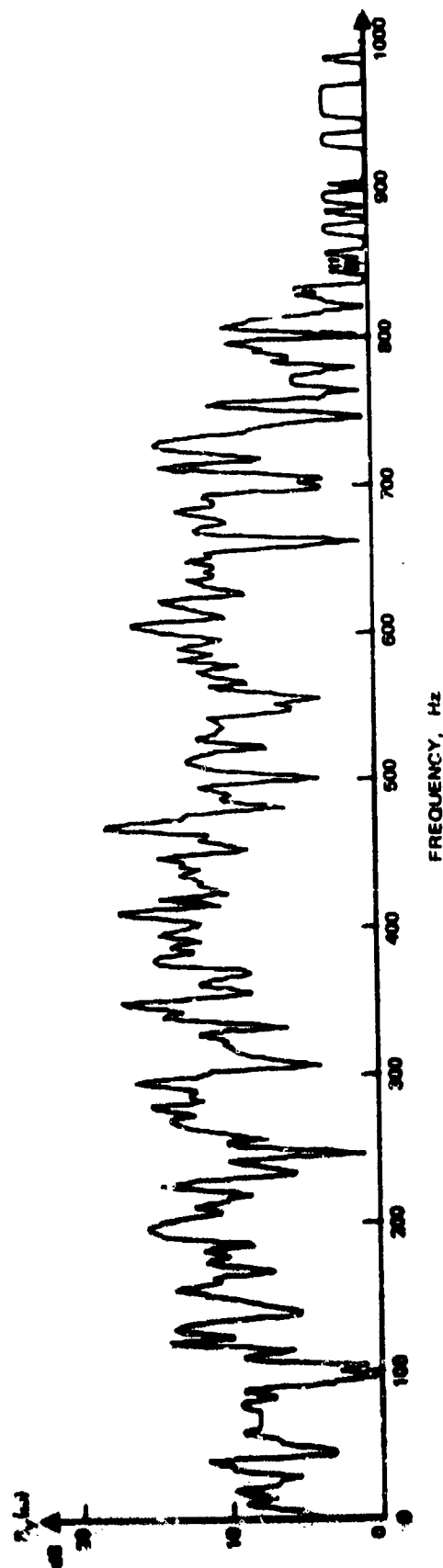Part B. 5 minutes after start of adaptation.

FREQUENCY, Hz

Figure 23. ALICE output power spectra for $\Delta = 200$ and $\mu_{ANC} = 2^{-10}$.

41

Part A. 1 minute after start of adaptation.

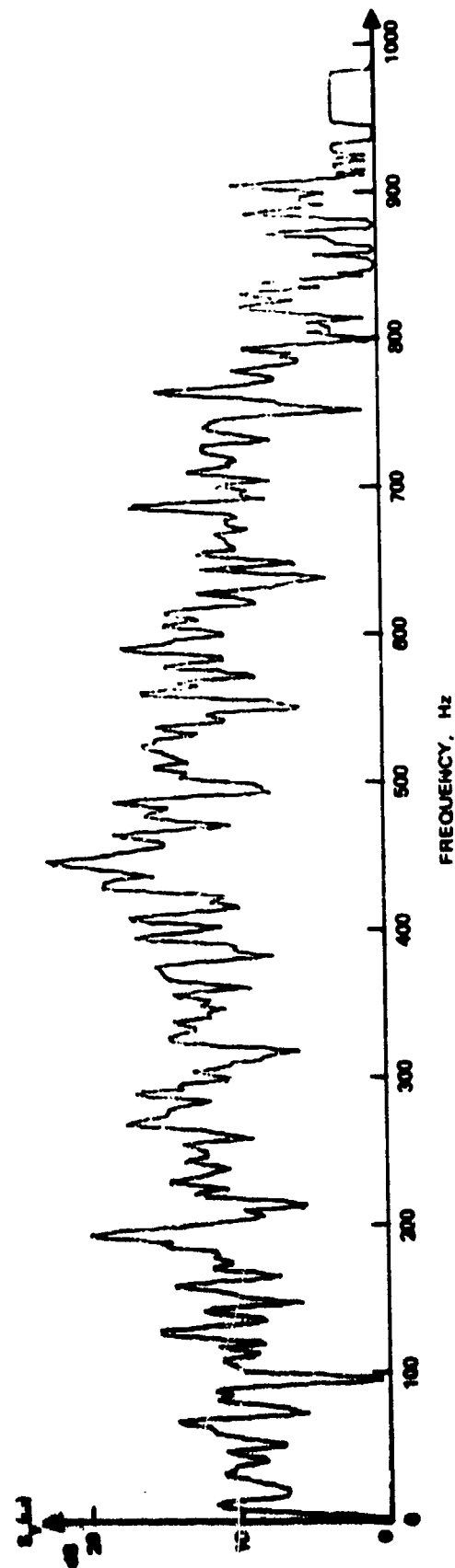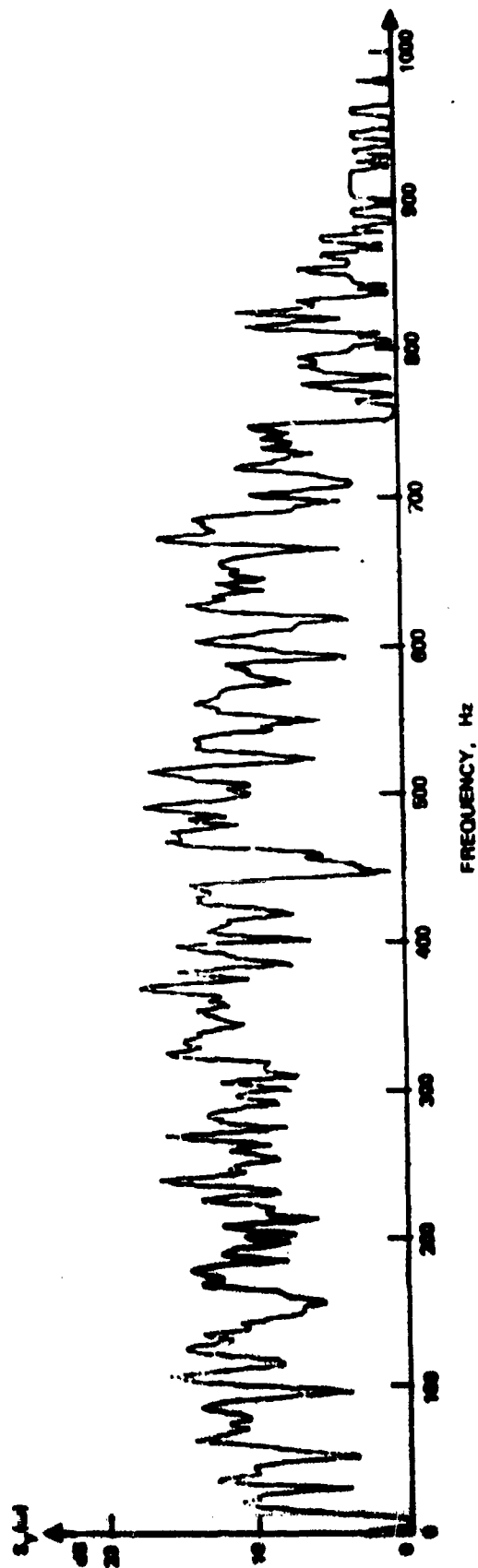Part B. 5 minutes after start of adaptation.

Figure 24. ALICE output power spectra for $\Delta = 500$ and $\mu_{ANC} = 2^{-10}$.

Part A. 1 minute after start of adaptation.

FREQUENCY, Hz

Part B. 5 minutes after start of adaptation.

FREQUENCY, Hz

Figure 25. ALICE output power spectra for $\Delta = 1000$ and $\mu_{ANC} = 2^{-10}$.

43

Part A. 1 minute after start of adaptation.
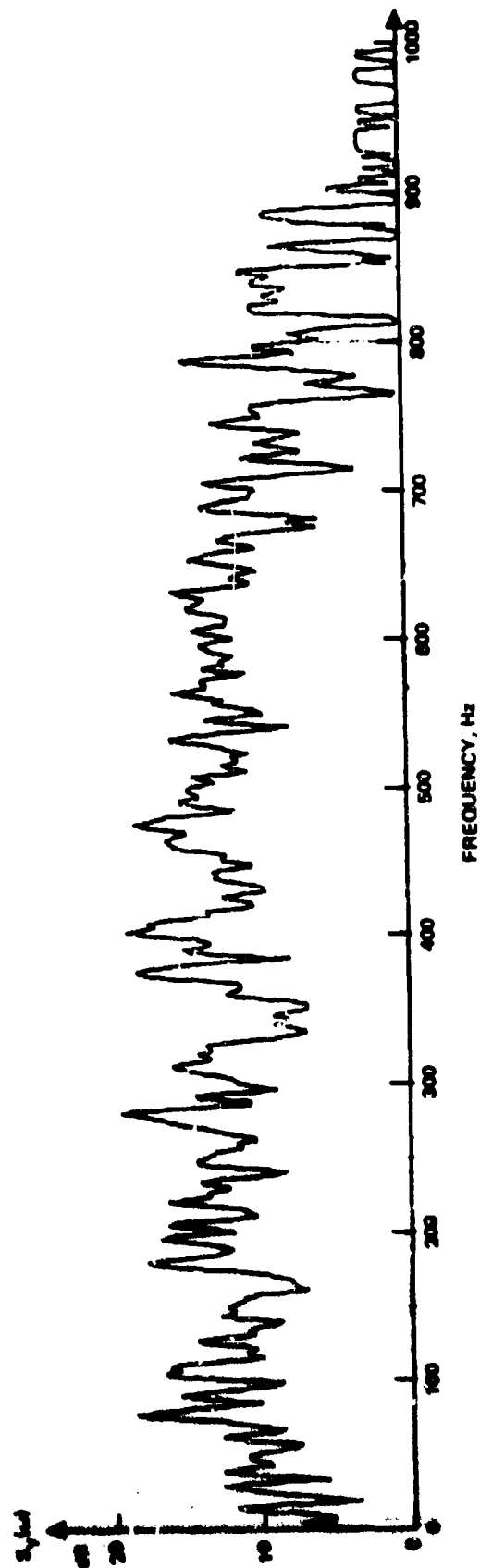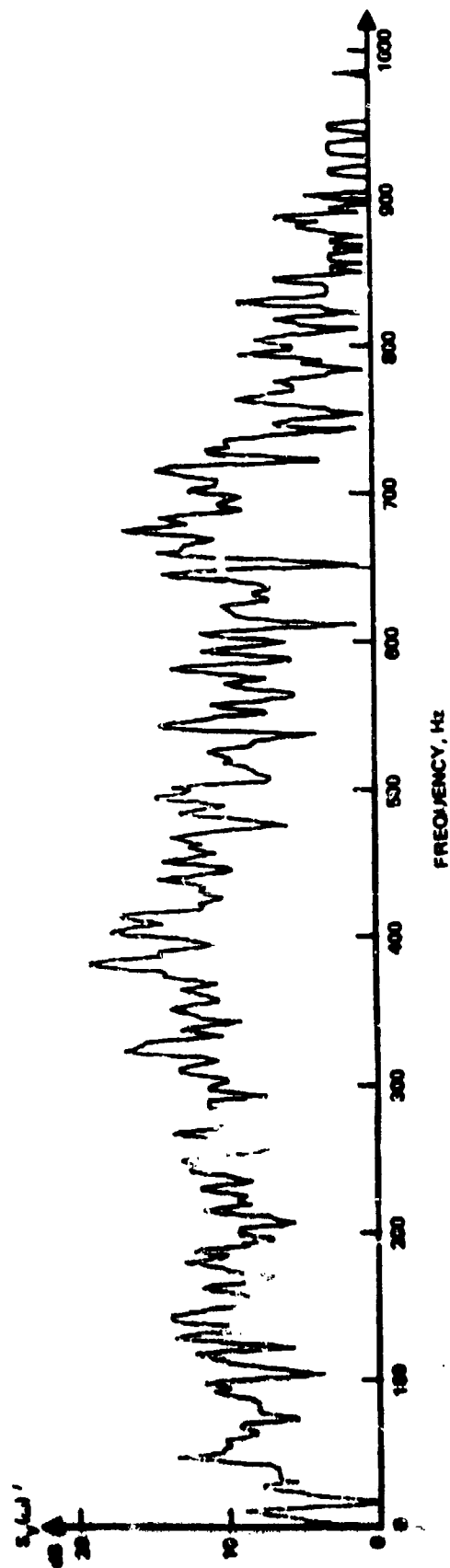
Part B. 5 minutes after start of adaptation.

Figure 26. ALICE output power spectra for $\Delta = 200$ and $\mu_{ANC} = 2^{-8}$.

44

Part A. 1 minute after start of adaptation.

Part B. 5 minutes after start of adaptation.
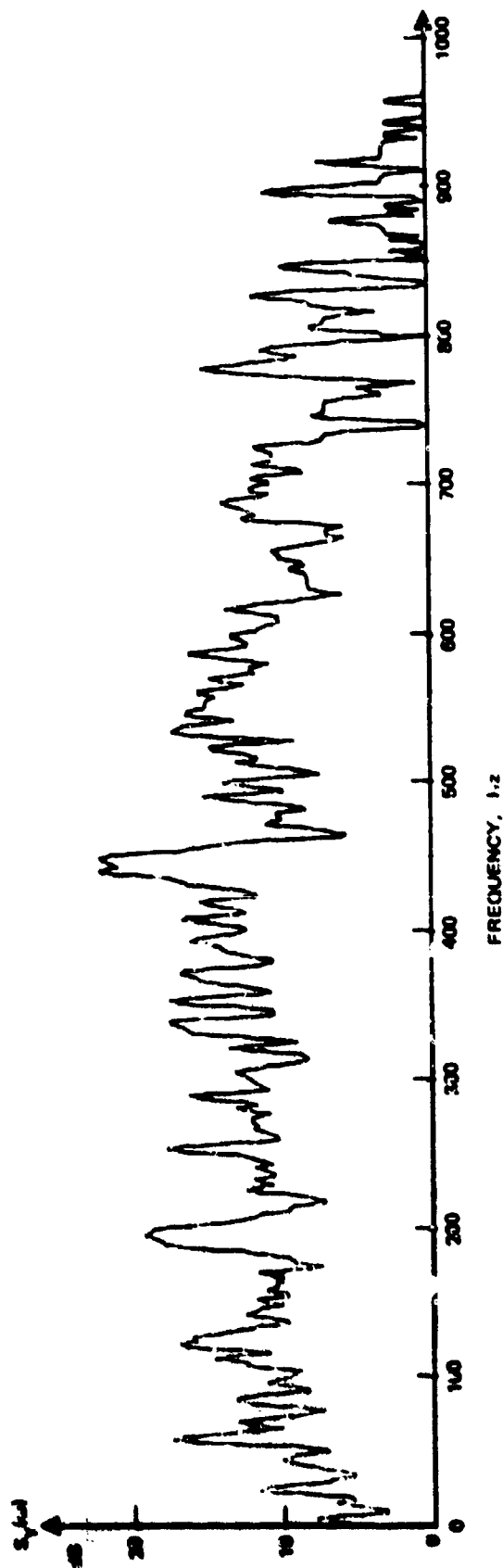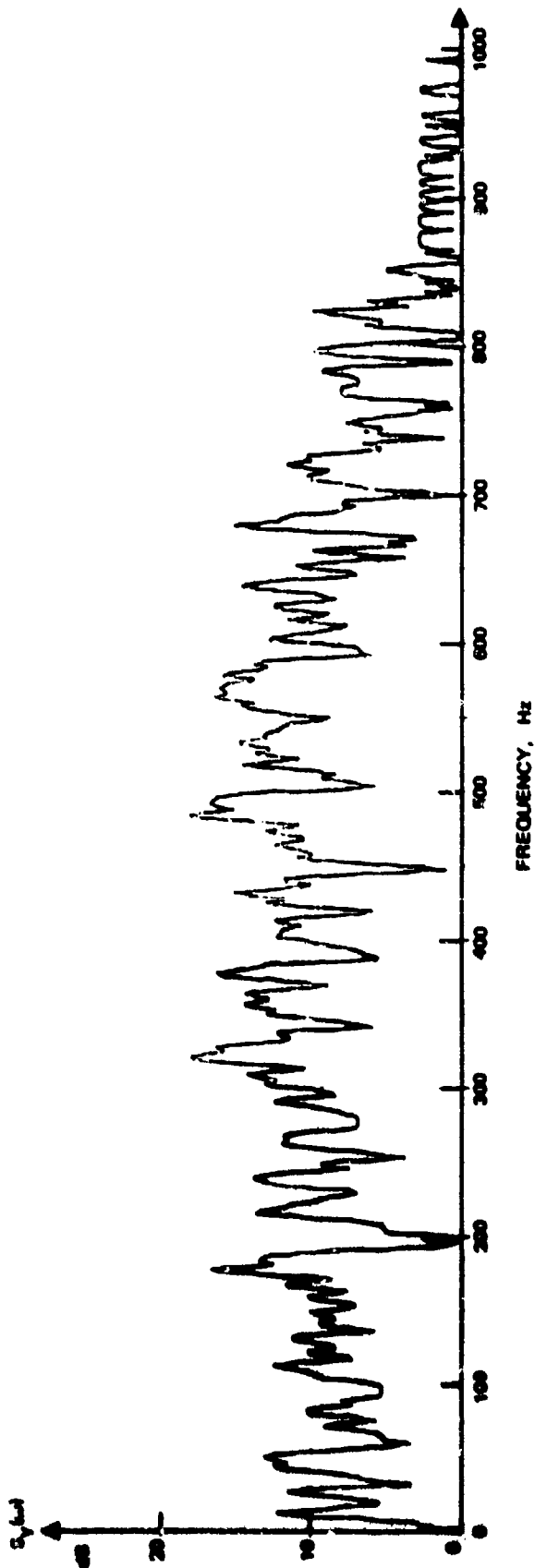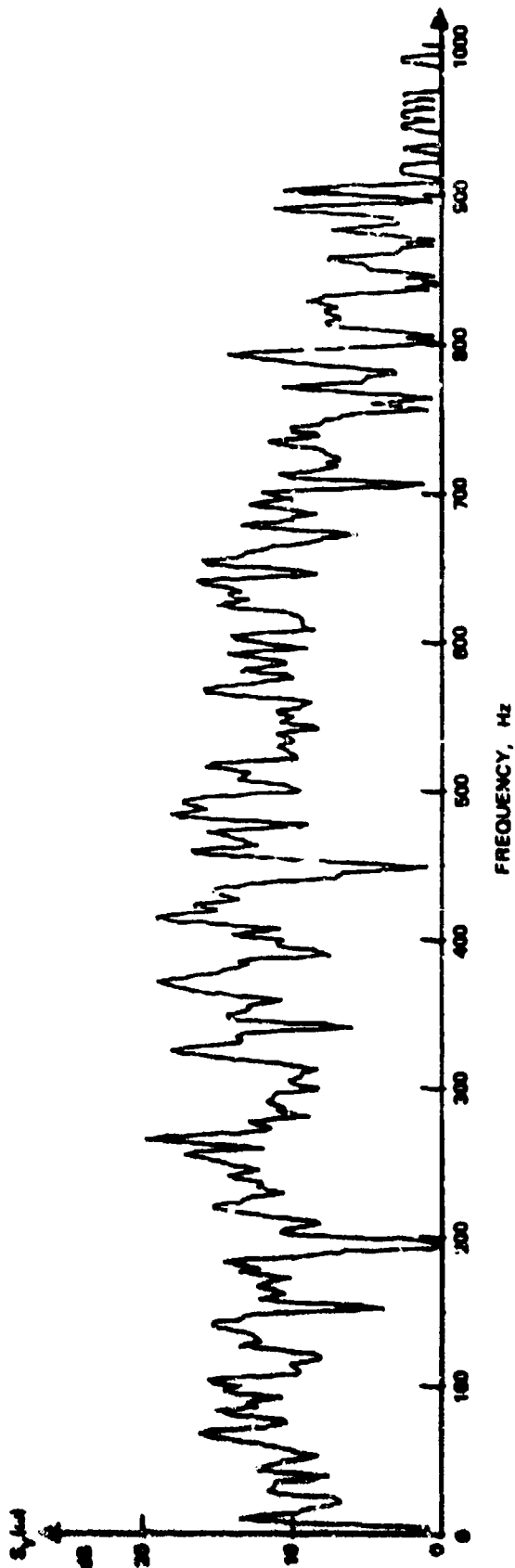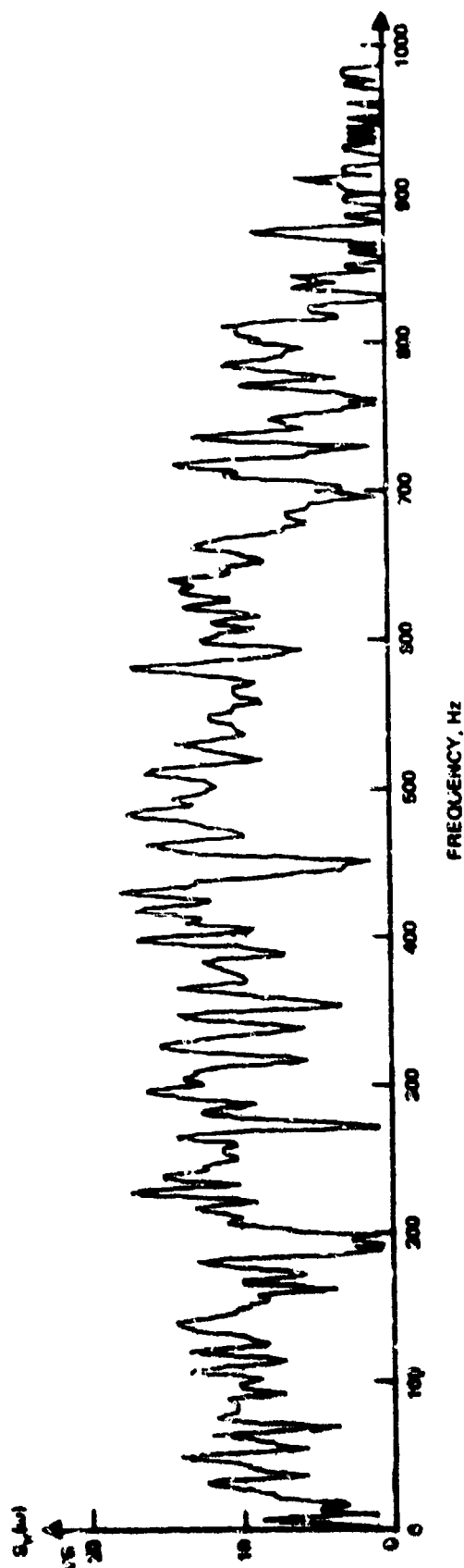
Figure 27. ALICE output power spectra for $\Delta = 500$ and $\mu_{ANC} = 2^{-8}$.

45

Part A. 1 minute after start of adaptation.

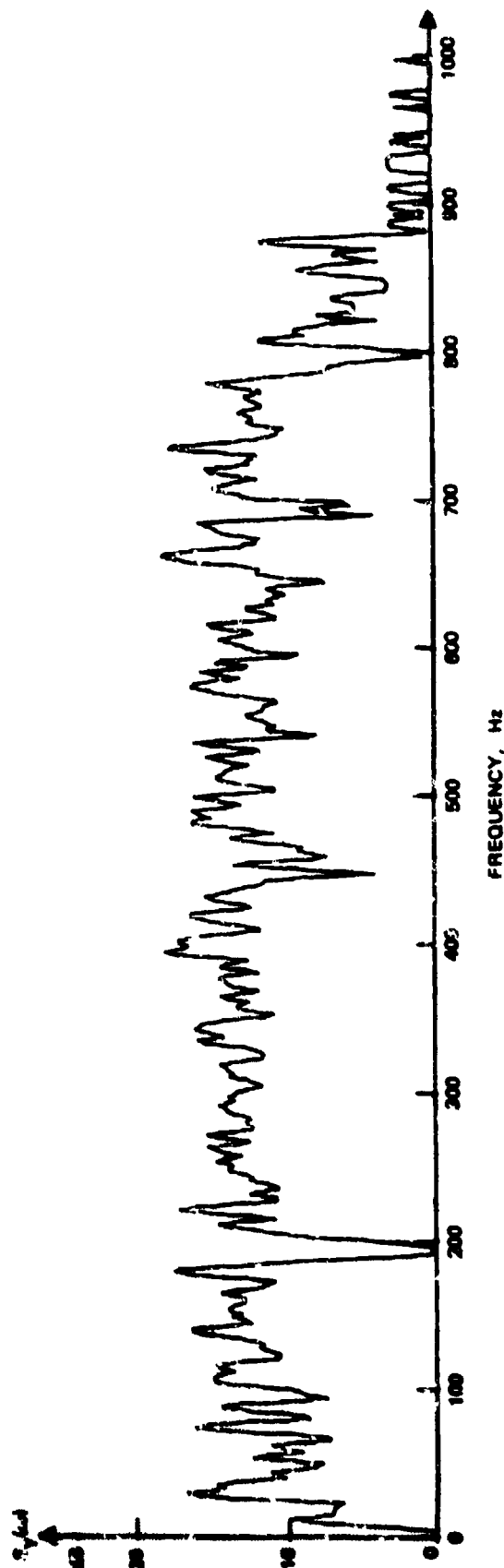Part B. 5 minutes after start of adaptation.

Figure 28. ALICE output power spectra for $\Delta = 1000$ and $\mu_{ANC} = 2^{-8}$.

46

CONCLUSIONS

In this report, the response of an ALE to a notched input spectrum was examined. In particular it was found that when the input to an ALE consisted of a notch in flat noise, the steady-state ALE output spectrum contained a peak at the notch frequency. In general, the ALE response time to the notch was much longer than the ALE response time to a signal. However, once the peak in the ALE output power spectrum appeared at the notch frequency, its presence could interfere with the detection of other signal peaks. Therefore, different methods of eliminating the peak were examined. It was found that increasing the ALE delay would decorrelate the notch and thus eliminate the undesirable peak. It was also found that by increasing the notch width, the peak could be eliminated. Another method included the addition of uncorrelated noise to the ALE input. Experimental data indicated the validity of these analyses.

REFERENCES

1. J. Glover, "Adaptive noise cancelling of sinusoidal interference," Naval Undersea Center, San Diego, California, Technical Note 1617, December 1975

2. B. Widrow, J. Glover, J. McCool, et al. "Adaptive noise cancelling: Principles and applications," *Proc. IEEE*, vol. 63, pp. 1692-1716, December 1975

3. J. Treichler, "The spectral line enhancer," Ph.D. Dissertation, Department of Electrical Engineering, Stanford University, Stanford, California, May 1977

4. J. Zeidler and D. Chabries, "An analysis of the LMS adaptive filter used as a spectral line enhancer," Naval Undersea Center, San Diego, California, Technical Publication 556, February 1975

5. Available to qualified requestors

6. Available to qualified requestors

7. B. Widrow, J. McCool, M. Larimore, and C. Johnson, Jr., "Stationary and nonstationary learning characteristics of the LMS adaptive filter," *Proc. IEEE*, vol. 64, pp. 1151-1162, August 1976

8. B. Widrow, "Adaptive filters," *Aspects of Network and System Theory*, R. Kalman and N. DeClaris, editors, New York: Holt, Rhinehart, and Winston, 1971, pp. 563-587

9. L. Griffiths, "Rapid measurement of digital instantaneous frequency," *IEEE Trans. Acous., Speech, and Sig. Proc.*, vol. ASSP-23, pp. 209-222, April 1975

10. R. Keeler and L. Griffiths, "Acoustic Doppler extraction by adaptive linear prediction filtering," *J. Acous. Soc. Amer.*, vol. 61, pp. 1218-1227, May 1977

11. J. Zeidler, E. Satorius, D. Chabries, and H. Wexler, "Adaptive enhancement of multiple sinusoids in uncorrelated noise," *IEEE Trans. Acous., Speech, and Sig. Proc.* (in publication)

12. D. Morgan and S. Craig, "Real-time linear prediction using the least mean square gradient algorithm," *IEEE Trans. Acous., Speech, and Sig. Proc.*, vol. ASSP-24, pp. 494-507, December 1976

13. M. Lighthill, *Introduction to Fourier Analysis and Generalized Functions*, Cambridge University Press: New York, 1959

14. B. Widrow, P. Mantey, L. Griffiths, and B. Goode, "Adaptive antenna systems," *Proc. IEEE*, vol. 55, pp. 2143-2159, December 1967

15. E. Satorius and J. Zeidler, "Least-mean-square, finite length, predictive digital filters," *Conference Record of the IEEE International Conference on Acoustics, Speech and Signal Processing*, Hartford, Connecticut. May 9-11, 1977

16. K. Peacock and S. Treitel, "Predictive deconvolution: Theory and practice," *Geophysics*, vol. 34, pp. 155-169, April 1969

17. J. Makhoul, "Linear prediction: A tutorial review," *Proc. IEEE*, vol. 63, pp. 561-580, April 1975

18. T. Kailath, "A view of three decades of linear filtering theory," *IEEE Trans. Inform. Theory*, vol. IT-20, pp. 145-181, March 1974

19. J. Treichler, "Private Communication," June 1977

20. S. Alexander, "The ALE output convariance function for a sinusoid in uncorrelated noise," Naval Ocean Systems Center, San Diego, California, Technical Report (in publication)

21. L. Griffiths, J. Keeler, R. Medaugh, "Detection and convergence results relating to the performance of an Adaptive Line Enhancer," Naval Undersea Center, San Diego, California, Technical Note 1831, December 1976